Available online at www.sciencedirect.com
ScienceDirect
Journal of Sound and Vibration 309 (2008) 375–406
JOURNAL OF SOUND AND VIBRATION
www.elsevier.com/locate/jsvi

Nonlinear dynamics of a pipe conveying pulsating fluid with combination, principal parametric and internal resonances

L.N. Panda[a,*], R.C. Kar[b,1]

[a]Department of Mechanical Engineering, College of Engineering and Technology, Biju Patnaik University of Technology, Bhubaneswar, India
[b]Department of Mechanical Engineering, Indian Institute of Technology, Kharagpur 721302, India

Received 10 June 2006; received in revised form 5 January 2007; accepted 13 May 2007
Available online 22 October 2007

Abstract

Nonlinear dynamics of a hinged–hinged pipe conveying pulsatile fluid subjected to combination and principal parametric resonance in the presence of internal resonance is investigated. The system has geometric cubic nonlinearity due to stretching effect out of immovable support conditions at both ends. The pipe conveys fluid at a velocity with a harmonically varying component over a constant mean velocity. For appropriate choice of system parameters, the natural frequency of the second mode is approximately three times that of the first mode for a range of mean flow velocity, activating a three-to-one internal resonance. The analysis is carried out using the method of multiple scales by directly attacking the governing nonlinear integro-partial-differential equations and the associated boundary conditions. The set of first-order ordinary differential equations governing the modulation of amplitude and phase is analyzed numerically for combination parametric resonance and principal parametric resonance. Stability, bifurcation and response behavior of the pipe are investigated. The amplitude and frequency detuning of the harmonic velocity perturbation are taken as the control parameters. The system exhibits response in the directly excited and indirectly excited modes due to modal interaction. Dynamic response of the system is presented in the form of phase plane trajectories, Poincare maps and time histories. A wide array of dynamical behavior is observed illustrating the influence of internal resonance.
© 2007 Elsevier Ltd. All rights reserved.

1. Introduction

There are a number of practical applications involving fluid–structure interactions, notable among which are the pipes conveying fluid. Pipes with internal fluid-flow are found in many engineering installations, particularly in the power-generating, chemical and petrochemical industries in the form of process piping, heat exchanger tube bundles, hydraulic oil tubes and lubrication pipes. These structures are subjected to flow-induced vibration due to turbulence in the flow or due to resonance with some periodicity in the flow, which may itself arise by fluid–structure interaction. At sufficiently high flow velocities, these are subjected to self-excited fluidelastic instabilities like divergence and flutter. These flow-induced instabilities, in addition to being

*Corresponding author.
E-mail address: lnpanda@yahoo.com (L.N. Panda).
[1]Former Professor.

0022-460X/$ - see front matter © 2007 Elsevier Ltd. All rights reserved.
doi:10.1016/j.jsv.2007.05.023

of practical concern, are of immense fundamental interest in illustrating the phenomenon of structural stability and the underlying mechanisms.

The subject of pipes conveying fluid has been studied extensively over a long period of time. Due to a number of factors like parametric excitation in the form of flow fluctuation, external excitations, support conditions, articulated or continuous nature of pipe, additional system configurations like lumped mass, attached nozzles, elastic foundations, elastic constraints and different forms of nonlinearities in the system arising from various sources, the system exhibits a wide array of dynamical behavior. The linear and nonlinear dynamics of pipes conveying fluid has thus been a subject of widespread research over the last four decades. Paidoussis et al. [1–3] provided detailed review and extensive bibliography on this diverse and interesting flow-induced vibrations and instabilities of pipings and cylindrical structures, projecting the subject as a model dynamical problem. These reviews discussed various aspects like mathematical modeling, solution methodology, effect of system parameters like boundary conditions, fluid pipe mass ratio, gravity effect, parametric instabilities of the system due to pulsatile flow, fluid friction effects, the mechanisms of instabilities, destabilizing effects of dissipation, effects of elastic constraints, motion limiting constraints, lumped mass, attached nozzles, elastic foundation and various other parameters on the dynamics of the system.

When the flow velocity has a harmonically fluctuating component over a mean value, the pipe experiences parametric instabilities depending on the amplitude and frequency of flow fluctuation. Detailed investigations based on linearized analytical models of these parametric instability problems for simply supported pipes were done by Chen [4], Paidoussis and Issid [5], Paidoussis and Sundararajan [6], Ginsberg [7] and Ariaratnam and Namachchivaya [8]. They studied the parametric and combination resonances and evaluated instability regions using numerical methods, viz., Bolotin's method and numerical Floquet analysis. Various other authors considered nonlinear pipes conveying pulsating fluid, notably due to Namachchivaya [9], Namachchivaya and Tien [10], Jayaraman and Narayanan [11], Chang and Chen [12] and Yoshizawa et al. [13]. Some other notable contributions in the nonlinear dynamics of pipes conveying fluid at steady flow-velocity are by Thurman and Mote [14], Holmes [15], Holmes and Marsden [16], Rousselet and Hermann [17], Bajaj et al. [18] and Bajaj and Sethna [19,20].

The problem of pipes conveying fluid belongs to the broader class of problems involving axially moving continua, as in other applications like traveling beam and analysis carried out in similar lines. Analysis of such problems involving linear and nonlinear models exist in the literature. Some papers concern systems with constant velocity and others deal with time-dependent velocity. Transverse vibrations of tensioned pipes conveying fluid with time-dependent velocity and with vanishing flexural stiffness was studied by Oz and Boyaci [21]. Solution of the integro-differential equation of motion was obtained by direct application of the perturbation technique (MMS) in contrast to the discretization perturbation technique. Calculation of natural frequency for this system of traveling continua was done by complex analysis taking fluid velocity and the fluid-pipe mass ratio as parameters and stability charts for principal parametric resonances presented. Oz [22] extended the work considering nonlinear effects due to stretching of the neutral axis but using similar approach as previous. Stability and bifurcation analysis for both trivial and nontrivial state was carried out and frequency response plots presented. Oz et al. [23] considered another problem belonging to this broader class of axially moving continua, viz. nonlinear traveling beam with pulsating speed through direct perturbation (MMS) technique and carried out a stability analysis. The direct perturbation technique has been used considering its advantage over the discretization perturbation method [24–26]. Modal interactions in multi-degree-of-freedom systems or continuous systems are dealt in Refs. [27–30]. Due to commensurable relationships of the frequencies of the system for specific values of the system parameters, internal resonance occurs influencing the system behavior under external or parametric excitation through energy exchange among the interacting modes.

From the review of literature, it is found that the study of internal resonance in the area of flow induced vibration in pipes conveying fluid has not yet been explored so far. The nonlinear modal interaction or the internal resonance in the system arising out of commensurable relationships of frequencies, in presence of parametric excitation due to pulsatile flow can have possible influence on system behavior, which needs to be studied.

In the present paper, we analyze the nonlinear planar vibration of a hinged–hinged pipe conveying fluid with harmonic flow velocity pulsation in the presence of internal resonance. Geometric cubic nonlinear terms are included in the equation of motion due to midline stretching of the pipe.

The linear natural frequencies of the system are dependent on the mean flow velocity besides other system parameters and for a particular range of the flow velocity, the natural frequency of the second mode is approximately three times that of the first providing the condition for 3:1 internal resonance. It is worth noting that in a conventional hinged–hinged beam involving classical normal modes, although there are commensurable linear natural frequencies, there are no internal resonances because of the vanishing of the coupling coefficients leading to internal resonance and consequently only directly excited modes are present [31]. In contrast, in this study it is demonstrated that for the pipes conveying fluid with similar boundary conditions, the modal coupling coefficients do not vanish and internal resonance exists. Hence internal resonance, in conjunction with parametric resonances in the system due to the parametric excitation related to flow pulsation is considered.

Principal parametric resonance of second mode and combination parametric resonance of sum type are considered here. Principal parametric resonance of first mode which also simultaneously activates a combination parametric resonance of difference type in presence of 3:1 internal resonance is not considered here due to lack of space and is studied in another paper.

Adopting the direct perturbation MMS technique, the partial differential equation of motion of the pipe is reduced to sets of first-order nonlinear modulation equations in terms of the complex modes of the pipe. These modulation equations are numerically analyzed for stability and bifurcations of trivial and nontrivial solutions. Bifurcation diagrams representing system responses with variation of parameters like amplitude and frequency of flow pulsation, frequency detuning of internal resonances and damping are computed with the help of a continuation algorithm [32]. The trivial state stability plots are presented. The modulation equations are also numerically integrated to obtain the dynamic solutions viz periodic, quasiperiodic and chaotic responses for typical system parameters.

For the principal parametric resonance of second mode, the influence of internal resonance is illustrated in the form of two mode solutions in the frequency and amplitude responses, which coexist with the trivial and single-mode solutions. The system is shown to have pitchfork bifurcations, Hopf bifurcations and saddle node bifurcations for different parameter values. The influence of intensity of flow pulsation and frequency detuning for internal resonance on the strength of nonlinear modal interaction are illustrated. The system is shown to exhibit dynamic solutions like periodic and quasiperiodic responses for typical range of parameter values.

For the combination parametric resonance, the system is shown to have two mode solution coexisting with the trivial state. The system exhibits saddle node and Hopf bifurcations and dynamic solutions like periodic, quasiperiodic and chaotic responses with variation of parameters. The chaos is shown to occur through quasiperiodic route. The phase planes, time spectra, power spectra and Poincare sections are presented, which are illustrative of the dynamic behavior.

2. Formulation of the problem

We consider a uniform horizontal pipe hinged at both ends conveying fluid with a flow-velocity having a harmonically pulsating component superimposed over a steady one (Fig. 1). It is assumed that the motion is planar and the uniform cross-section remains plane during the motion and the tube behaves like an Euler–Bernoulli beam in transverse vibration. The fluid is assumed to be incompressible and has plug flow conditions. The equation of transverse motion of the pipe including the nonlinearity due to midline stretching

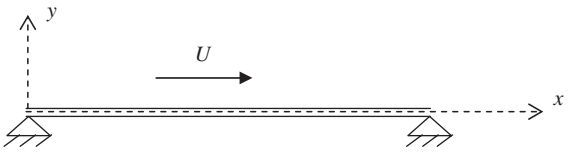

Fig. 1. Schematics of the hinged–hinged pipe.

is given by Paidoussis [1]:

$$EI\frac{\partial^4 y}{\partial x^4}+E^*I\frac{\partial^5 y}{\partial x^4\partial t}+2MU\frac{\partial^2 y}{\partial x\partial t}+(M+m)\frac{\partial^2 y}{\partial t^2}+c\frac{\partial y}{\partial t}$$
$$+\left[MU^2-\bar{T}+M\frac{\partial U}{\partial t}(L-x)-\frac{EA}{2L}\int_0^L (y')^2\,\mathrm{d}x-\frac{E^*A}{L}\int_0^L (y'\dot{y}')\,\mathrm{d}x\right]\frac{\partial^2 y}{\partial x^2}=0, \tag{1}$$

with the associated boundary conditions

$$y(0,t)=y(L,t)=\frac{\partial^2 y}{\partial x^2}(0,t)=\frac{\partial^2 y}{\partial x^2}(L,t)=0, \tag{2}$$

where x is the longitudinal coordinate, y represents the transverse deflection, U is the fluid velocity, $\bar{T}$ is the externally imposed axial tension, m and M are respectively the mass per unit length of pipe and fluid materials, A is the cross sectional area of the pipe, L is the length, EI is the flexural stiffness of the pipe material, E^* is the coefficient of internal dissipation of the pipe material which is assumed to be viscoelastic and of the Kelvin–Voigt type and c is the external damping factor. Assuming the harmonic flow fluctuation of the form

$$U=U_0(1+v\sin\omega t), \tag{3}$$

where U_0 is the mean flow velocity and v and ω are the amplitude and frequency of the flow–velocity fluctuation. This fluctuating flow velocity appears as parametric excitation term in the equation of motion leading to parametric instabilities.

Incorporating the following dimensionless quantities

$$\xi=\frac{x}{L},\quad w=\frac{y}{L},\quad \tau=\frac{1}{L^2}\left(\frac{EI}{M+m}\right)^{1/2}t=\omega_n t,\quad u=\left(\frac{M}{EI}\right)^{1/2}UL,$$
$$\beta=\frac{M}{m+M},\quad \Gamma=\frac{\bar{T}L^2}{EI},\quad \sigma^*=\frac{cL^2}{\sqrt{EI(M+m)}},$$
$$\alpha^*=\frac{E^*}{L^2}\left\{\frac{I}{(M+m)E}\right\}^{1/2},\quad k=\frac{AL^2}{2I},\quad \Omega=\frac{\omega}{\omega_n},\quad \delta^*=\frac{E^*A}{\sqrt{EI(M+m)}}, \tag{4}$$

the equation of motion can be nondimensionalized as

$$\alpha^* w''''+w''''+\left\{u^2-\Gamma+\beta^{1/2}\dot{u}(1-\xi)\right\}w''+2\beta^{1/2}u\dot{w}'+\sigma^*\dot{w}+\ddot{w}$$
$$-k\int_0^1 w'^2\,\mathrm{d}\xi w''-\delta^*\int_0^1 w'\dot{w}'\,\mathrm{d}\xi w''=0, \tag{5}$$

$$u=u_0(1+v\sin\Omega\tau), \tag{6}$$

The primes and dots represent differentiation with respect to nondimensional longitudinal coordinate ξ and nondimensional time τ. To express the smallness of the amplitude of motion w, we scale it with the factor $\varepsilon^{1/2}$, where the small parameter ε is a measure of amplitude and is also used as a book keeping device in the subsequent perturbation analysis. Introducing this scaling factor and using Eq. (6) for pulsating flow velocity, the nondimensional equation of motion becomes

$$w''''+\left[u_0^2+2\varepsilon u_0u_1\sin\Omega\tau-\Gamma\right]w''+\sqrt{\beta}\varepsilon u_1\Omega\cos\Omega\tau(1-\xi)w''$$
$$+2\sqrt{\beta}(u_0+\varepsilon u_1\sin\Omega\tau)\dot{w}'+2\varepsilon\mu\dot{w}+2\varepsilon\alpha\dot{w}''''+\ddot{w}$$
$$=\varepsilon k\int_0^1 w'^2\,\mathrm{d}\xi w''+O(\varepsilon^2), \tag{7}$$

with the boundary conditions

$$w(0,\tau)=0,\quad w(1,\tau)=0,\quad w''(0,\tau)=0,\quad w''(1,\tau)=0, \tag{8}$$

where

$$\mu = \sigma^*/2\varepsilon, \quad \alpha = \alpha^*/2\varepsilon, \quad u_0 v = \varepsilon u_1. \tag{9}$$

As Eq. (7) contains cubic nonlinearity, it does not lend itself to closed-form solution. One can find the approximate solution using the perturbation techniques or some other numerical techniques.

3. Method of analysis

The present system of hinged–hinged pipe is analyzed in the form of a first-order uniform expansion through the MMS applied directly to the partial differential Eq. (7) and the associated boundary conditions (8). The direct perturbation technique has been used considering its advantage over the discretization-perturbation technique [24–26,30]. Though the direct perturbation method and the discretization-perturbation method, both for linear and nonlinear systems, yield identical results for infinite modes, the former gives better results for finite mode truncation if a higher order perturbation scheme were used. For lower order perturbation schemes, as adopted in the present case, both methods yield identical results. But the choice of orthogonal basis functions for the discretization-perturbation equation might not be so straightforward for some involved cases and a transformation of equation to a convenient form for orthogonalizing the modes may be needed. In such a case, employing the direct perturbation method would be more straightforward, even though the algebra might be more involved.

We seek an approximate solution to this weakly nonlinear distributed parameter system in the form of a first-order uniform expansion and introduce the time scale $T_n = \varepsilon^n \tau$, $n = 0,1,2,\ldots$. The time derivatives are

$$\frac{\mathrm{d}}{\mathrm{d}\tau} = D_0 + \varepsilon D_1 + \ldots, \quad \frac{\mathrm{d}^2}{\mathrm{d}\tau^2} = D_0^2 + 2\varepsilon D_0 D_1 + \ldots, D_n = \partial/\partial T_n, \quad n = 0, 1, 2, \ldots. \tag{10}$$

We write the expansion of $w(\xi,\tau)$ in the form

$$w(\xi, \tau) = w_1(T_0, T_1, \xi) + \varepsilon w_2(T_0, T_1, \xi) + \cdots \tag{11}$$

Substituting Eqs. (10) and (11) into Eqs. (7) and (8) and equating coefficients of like powers of ε on both sides, we obtain

$$\begin{aligned} O(\varepsilon^0): \; & D_0^2 w_0 + 2\sqrt{\beta} u_0 D_0 w_0' + (u_0^2 - \Gamma) w_0'' + w_0'''' = 0 \\ & w_0(0,\tau) = w_0(1,\tau) = w_0''(0,\tau) = w_0''(1,\tau) = 0, \end{aligned} \tag{12}$$

$$\begin{aligned} O(\varepsilon^1): \; & D_0^2 w_1 + 2\sqrt{\beta} u_0 D_0 w_1' + (u_0^2 - \Gamma) w_1'' + w_1'''' \\ & = -2D_0 D_1 w_0 - 2\alpha D_0 w_0'''' - 2\mu D_0 w_0 - 2\sqrt{\beta} u_0 D_1 w_0' - 2\sqrt{\beta} u_1 \sin \Omega T_0 \times D_0 w_0' \\ & \quad - \sqrt{\beta} u_1 \Omega \cos \Omega T_0 (1 - \xi) w_0'' - 2\sqrt{\beta} u_0 u_1 \sin \Omega T_0 \times D_0 w_0' + k w_0'' \int_0^1 w_0'^2 \, \mathrm{d}x \\ & w_1(0,\tau) = w_1(1,\tau) = w_1''(0,\tau) = w_1''(1,\tau) = 0 \end{aligned} \tag{13}$$

The solution of Eq. (12) can be expressed as

$$w_0(T_0, T_1, \xi) = \sum_{m=1}^{\infty} \phi_m(\xi) A_m(T_1) \, \mathrm{e}^{\mathrm{i}\omega_m T_0} + cc, \tag{14}$$

where $\phi_m(\xi)$ are the mode shapes, ω_m are the natural frequencies and cc stands for complex conjugate. The mode shapes $\phi_m(\xi)$ for the specified hinged–hinged boundary conditions are calculated as

$$\begin{aligned} \phi_m(\xi) = C_{1m} \Bigg\{ & \mathrm{e}^{\mathrm{i}\beta_{1m}\xi} - \frac{(\beta_{4m}^2 - \beta_{1m}^2)(\mathrm{e}^{\mathrm{i}\beta_{3m}} - \mathrm{e}^{\mathrm{i}\beta_{1m}})}{(\beta_{4m}^2 - \beta_{2m}^2)(\mathrm{e}^{\mathrm{i}\beta_{3m}} - \mathrm{e}^{\mathrm{i}\beta_{2m}})} \mathrm{e}^{\mathrm{i}\beta_{2m}\xi} - \frac{(\beta_{4m}^2 - \beta_{1m}^2)(\mathrm{e}^{\mathrm{i}\beta_{2m}} - \mathrm{e}^{\mathrm{i}\beta_{1m}})}{(\beta_{4m}^2 - \beta_{3m}^2)(\mathrm{e}^{\mathrm{i}\beta_{2m}} - \mathrm{e}^{\mathrm{i}\beta_{3m}})} \mathrm{e}^{\mathrm{i}\beta_{3m}\xi} \\ & + \left[-1 + \frac{(\beta_{4m}^2 - \beta_{1m}^2)(\mathrm{e}^{\mathrm{i}\beta_{3m}} - \mathrm{e}^{\mathrm{i}\beta_{1m}})}{(\beta_{4m}^2 - \beta_{2m}^2)(\mathrm{e}^{\mathrm{i}\beta_{3m}} - \mathrm{e}^{\mathrm{i}\beta_{2m}})} + \frac{(\beta_{4m}^2 - \beta_{1m}^2)(\mathrm{e}^{\mathrm{i}\beta_{2m}} - \mathrm{e}^{\mathrm{i}\beta_{1m}})}{(\beta_{4m}^2 - \beta_{3m}^2)(\mathrm{e}^{\mathrm{i}\beta_{2m}} - \mathrm{e}^{\mathrm{i}\beta_{3m}})} \right] \mathrm{e}^{\mathrm{i}\beta_{4m}\xi} \Bigg\}, \end{aligned} \tag{15}$$

where β_{im} are the eigenvalues which satisfy the relation

$$\beta_{im}^4 + (\Gamma - u_0^2)\beta_{im}^2 - 2\sqrt{\beta}\omega_m u_0 \beta_{im} - \omega_m^2 = 0, \quad i = 1,2,3,4 \tag{16}$$

and the characteristic equation

$$\begin{aligned}&\left[e^{i(\beta_{1n}+\beta_{2n})} + e^{i(\beta_{3n}+\beta_{4n})}\right](\beta_{1n}^2 - \beta_{2n}^2)(\beta_{3n}^2 - \beta_{4n}^2)\\ &+ \left[e^{i(\beta_{1n}+\beta_{3n})} + e^{i(\beta_{2n}+\beta_{4n})}\right](\beta_{2n}^2 - \beta_{4n}^2)(\beta_{3n}^2 - \beta_{1n}^2)\\ &+ \left[e^{i(\beta_{2n}+\beta_{3n})} + e^{i(\beta_{1n}+\beta_{4n})}\right](\beta_{1n}^2 - \beta_{4n}^2)(\beta_{2n}^2 - \beta_{3n}^2) = 0.\end{aligned} \tag{17}$$

The linear natural frequencies of the pipe conveying fluid vary with the mean flow-velocity for different modes for variation of parameters like flexural stiffness, fluid-pipe mass ratio and axial tension. For specific combinations of system parameters, the lower natural frequencies can be commensurable, leading to internal resonance in the system and nonlinear interaction between the associated modes. We analyze the specific case of two mode interaction corresponding to particular system parameters. A three-to-one internal resonance $\omega_2 \approx 3\omega_1$ is considered for a range of mean flow velocity u_0 and it is assumed that there is no other commensurable frequency relationship with higher modes. We analyze the cases of principal parametric and combination parametric resonances involving the first two modes, for subcritical flow velocities. Since none of these first two modes is in internal resonance with any other mode of the tube, all other modes except the directly or indirectly excited first or second mode decay with time due to the presence of damping and the first two modes will contribute to the long term system response [30,31]. Hence we can replace Eq. (14) by

$$w_0(T_0, T_1, \xi) = A_1(T_1)\phi_1(\xi)e^{i\omega_1 T_0} + A_2(T_1)\phi_2(\xi)e^{i\omega_2 T_0} + cc, \tag{18}$$

Next we consider the cases of principal parametric resonance of second mode and combination parametric resonance of sum type. The difference type combination resonance $\Omega \approx \omega_2 - \omega_1$ in presence of 3:1 internal resonance ($\omega_2 \approx 3\omega_1$) is simultaneously activated when we consider principal parametric resonance of first mode ($\Omega \approx 2\omega_1$) in conjunction with 3:1 internal resonance ($\omega_2 \approx 3\omega_1$), which is studied in another paper.

3.1. Principal parametric resonance

We consider the principal parametric resonance of second mode and describe the nearness of ω_2 to $3\omega_1$ and Ω to $2\omega_2$ using the detuning parameters σ_1 and σ_2. For this, we write the frequency relations for the internal resonance and principal parametric resonance of second mode as

$$\omega_2 = 3\omega_1 + \varepsilon\sigma_1 \quad \text{and} \quad \Omega = 2\omega_2 + \varepsilon\sigma_2, \tag{19}$$

Substituting Eqs. (18) and (19) into Eq. (13), we get

$$\begin{aligned}&D_0^2 w_1 + 2\sqrt{\beta}u_0 D_0 w_1' + (u_0^2 - \Gamma)w_1'' + w_1''''\\ &\quad = \Gamma_1 e^{i\omega_1 T_0} + \Gamma_2 e^{i(\omega_1 T_0 + \sigma_1 T_1)} + \Gamma_8 e^{i(\omega_2 T_0 + \sigma_2 T_1)}\\ &\quad + \Gamma_5 e^{i\omega_2 T_0} + \Gamma_6 e^{i(\omega_2 T_0 - \sigma_1 T_1)} + cc + NST\end{aligned} \tag{20}$$

where the terms Γ_n are defined in Appendix. NST stands for terms that do not produce secular or small divisor terms. As the homogeneous part of Eq. (20) with its associated boundary conditions has a nontrivial solution, the corresponding nonhomogeneous problem has a solution only if a solvability condition is satisfied [26]. This requires the right-hand side of Eq. (20) to be orthogonal to every solution of the adjoint homogeneous problem, which leads to the complex variable modulation equations for the amplitude and phase

$$2A_1' + 2\mu C_1 A_1 + 2\alpha e_1 A_1 + 8S_1 A_1^2 \bar{A}_1 + 8S_2 A_1 A_2 \bar{A}_2 + 8G_1 \bar{A}_1^2 A_2 e^{i\sigma_1 T_1} = 0, \tag{21}$$

$$2A_2' + 2\mu C_2 A_2 + 2\alpha e_2 A_2 + 8S_4 A_2^2 \bar{A}_2 + 8S_3 A_1 A_2 \bar{A}_1 + 8G_2 A_1^3 e^{-i\sigma_1 T_1} + 2H_6 \bar{A}_2 e^{i\sigma_2 T_1} = 0, \tag{22}$$

where prime denotes differentiation with respect to the slow time T_1 and S_i, H_i, G_i , C_i and e_i are defined in Appendix. Overbar indicates complex conjugate. The terms in the above equations involving the internal frequency detuning parameter σ_1 are the contributions of internal resonance in the system.

3.2. Combination parametric resonance

We write the frequency relations for the internal resonance and combination parametric resonance (sum type) as

$$\omega_2 = 3\omega_1 + \varepsilon\sigma_1 \quad \text{and} \quad \Omega = \omega_1 + \omega_2 + \varepsilon\sigma_2, \tag{23}$$

where σ_1 and σ_2 are the detuning parameters.

Substituting Eqs. (18) and (23) into Eq. (13), we get

$$\begin{aligned} &D_0^2 w_1 + 2\sqrt{\beta}u_0 D_0 w_1' + (u_0^2 - \Gamma)w_1'' + w_1'''' \\ &\quad = \Gamma_1 e^{i\omega_1 T_0} + \Gamma_2 e^{i(\omega_1 T_0 + \sigma_1 T_1)} + \Gamma_8 e^{i(\omega_1 T_0 + \sigma_2 T_1)} \\ &\quad + \Gamma_5 e^{i\omega_2 T_0} + \Gamma_6 e^{i(\omega_2 T_0 - \sigma_1 T_1)} + \Gamma_3 e^{i(\omega_2 T_0 + \sigma_2 T_1)} + cc + NST, \end{aligned} \tag{24}$$

where the terms Γ_n are defined in Appendix. Following similar arguments as in Section 3.1, Eq. (24) leads to the modulation equations.

$$2A_1' + 2\mu C_1 A_1 + 2\alpha e_1 A_1 + 8S_1 A_1^2 \bar{A}_1 + 8S_2 A_1 A_2 \bar{A}_2 + 8G_1 \bar{A}_1^2 A_2 e^{i\sigma_1 T_1} + 2H_4 \bar{A}_2 e^{i\sigma_2 T_1} = 0, \tag{25}$$

$$2A_2' + 2\mu C_2 A_2 + 2\alpha e_2 A_2 + 8S_4 A_2^2 \bar{A}_2 + 8S_3 A_1 A_2 \bar{A}_1 + 8G_2 A_1^3 e^{-i\sigma_1 T_1} + 2H_5 \bar{A}_1 e^{i\sigma_2 T_1} = 0. \tag{26}$$

The internal resonance in the system are illustrated by the terms in the above equations involving the internal frequency detuning parameter σ_1.

4. Stability and bifurcations

4.1. Principal parametric resonance

From the above complex valued modulation equations, the evolution of equilibrium solutions, their stability and bifurcation analysis are carried out for the two cases. For this we introduce the polar transformation for the complex amplitude A_n

$$A_n = \frac{1}{2} a_n e^{i\beta_n}, \tag{27}$$

where a_n and β_n are the real valued amplitude and phase. Substituting Eq. (27) into Eqs. (21) and (22) for the case of principal parametric resonance and separating real and imaginary parts, we get the *reduced* equations for the modulation of amplitude and phase

$$a_1' = -\mu C_{1R} a_1 - \alpha e_{1R} a_1 - S_{1R} a_1^3 - S_{2R} a_1 a_2^2 - G_{1R} a_1^2 a_2 \cos\gamma_1 + G_{1I} a_1^2 a_2 \sin\gamma_1, \tag{28}$$

$$\begin{aligned} a_2' = &-\mu C_{2R} a_2 - \alpha e_{2R} a_2 - S_{4R} a_2^3 - S_{3R} a_1^2 a_2 - G_{2R} a_1^3 \cos\gamma_1 - G_{2I} a_1^3 \sin\gamma_1 \\ &- H_{6R} a_2 \cos\gamma_2 + H_{6I} a_2 \sin\gamma_2, \end{aligned} \tag{29}$$

$$\begin{aligned} \gamma_1' = &\sigma_1 + 3\mu C_{1I} + 3\alpha e_{1I} + 3S_{1I} a_1^2 + 3S_{2I} a_2^2 + 3G_{1R} a_1 a_2 \sin\gamma_1 + 3G_{1I} a_1 a_2 \cos\gamma_1 \\ &- \mu C_{2I} - \alpha e_{2I} - S_{4I} a_2^2 - S_{3I} a_1^2 + G_{2R} \frac{a_1^3}{a_2} \sin\gamma_1 - G_{2I} \frac{a_1^3}{a_2} \cos\gamma_1 \\ &- H_{6R} \sin\gamma_2 - H_{6I} \cos\gamma_2, \end{aligned} \tag{30}$$

$$\gamma_2' = \sigma_2 + 2\,\mu C_{2I} + 2\,\alpha e_{2I} + 2\,S_{3I}a_1^2 + 2\,S_{4I}a_2^2 - 2\,G_{2R}\frac{a_1^3}{a_2}\sin\gamma_1 + 2\,G_{2I}\frac{a_1^3}{a_2}\cos\gamma_1 + 2\,H_{6R}\sin\gamma_2 + 2\,H_{6I}\cos\gamma_2, \tag{31}$$

where $\gamma_1 = \beta_2 - 3\beta_1 + \sigma_1 T_1$ and $\gamma_2 = \sigma_2 T_1 - 2\beta_2$.

The stability of the nontrivial state can be obtained by perturbing these polar modulation equations and checking the eigenvalues of the resulting Jacobian matrix.

To determine the stability of the nontrivial state, these equations are perturbed to obtain

$$\{\Delta a_1', \Delta a_2', \Delta\gamma_1', \Delta\gamma_2'\}^{\mathrm{T}} = [J_c]\{\Delta a_1, \Delta a_2, \Delta\gamma_1, \Delta\gamma_2\}^{\mathrm{T}}, \tag{32}$$

where T denotes transpose and $[J_c]$ is the Jacobian matrix whose eigenvalues determine the stability and bifurcations of the system. Though, for the non-trivial state, one can obtain the stability by this method, it is not possible for the trivial state, as the perturbed equation will not contain the perturbations $\Delta\gamma_1'$ and $\Delta\gamma_2'$ due to the presence of the coupled terms $a_1\gamma_1'$ and $a_2\gamma_2'$ in the reduced Eqs. (28)–(31). To circumvent this difficulty, an alternative Cartesian formulation is utilized. Accordingly, the complex amplitude A_n is expressed as

$$A_n = \frac{1}{2}\left[p_n(T_1) - iq_n(T_1)\right]\mathrm{e}^{\mathrm{i}\lambda_n(T_1)}, \tag{33}$$

Substituting into Eqs. (21) and (22), using the notations in the Appendix, carrying out algebraic manipulations and separating real and imaginary parts, we arrive at the *normalized reduced* equations or the *Cartesian form of modulation* equations

$$\begin{aligned} p_1' = {} & -\mu C_{1R}p_1 - \mu C_{1I}q_1 - \alpha e_{1R}p_1 - \alpha e_{1I}q_1 - S_{1R}(p_1^3 + p_1q_1^2) - S_{1I}(p_1^2q_1 + q_1^3) \\ & - S_{2R}(p_1p_2^2 + p_1q_2^2) - S_{2I}(q_1p_2^2 + q_1q_2^2) - \vartheta_1 q_1 \\ & - G_{1R}(p_1^2p_2 - p_2q_1^2 + 2p_1q_1q_2) + G_{1I}(2p_1q_1p_2 - p_1^2q_2 + q_1^2q_2), \end{aligned} \tag{34}$$

$$\begin{aligned} q_1' = {} & -\mu C_{1R}q_1 + \mu C_{1I}p_1 - \alpha e_{1R}q_1 + \alpha e_{1I}p_1 + S_{1I}(p_1^3 + p_1q_1^2) - S_{1R}(p_1^2q_1 + q_1^3) \\ & - S_{2R}(q_1p_2^2 + q_1q_2^2) + S_{2I}(p_1p_2^2 + p_1q_2^2) + \vartheta_1 p_1 \\ & + G_{1R}(2p_1q_1p_2 - p_1^2q_2 + q_1^2q_2) + G_{1I}(p_1^2p_2 - p_2q_1^2 + 2p_1q_1q_2), \end{aligned} \tag{35}$$

$$\begin{aligned} p_2' = {} & -\mu C_{2R}p_2 - \mu C_{2I}q_2 - \alpha e_{2R}p_2 - \alpha e_{2I}q_2 - S_{4R}(p_2^3 + p_2q_2^2) - S_{4I}(q_2^3 + p_2^2q_2) \\ & - S_{3R}(p_1^2p_2 + p_2q_1^2) - S_{3I}(p_1^2q_2 + q_1^2q_2) - \vartheta_2 q_2 - H_{6R}p_2 + H_{6I}q_2 \\ & - G_{2R}(p_1^3 - 3p_1q_1^2) + G_{2I}(q_1^3 - 3p_1^2q_1), \end{aligned} \tag{36}$$

$$\begin{aligned} q_2' = {} & -\mu C_{2R}q_2 + \mu C_{2I}p_2 - \alpha e_{2R}q_2 + \alpha e_{2I}p_2 - S_{4R}(q_2^3 + p_2^2q_2) + S_{4I}(p_2^3 + p_2q_2^2) \\ & - S_{3R}(p_1^2q_2 + q_1^2q_2) + S_{3I}(p_1^2p_2 + p_2q_1^2) + \vartheta_2 p_2 + H_{6R}q_2 + H_{6I}p_2 \\ & + G_{2R}(q_1^3 - 3p_1^2q_1) + G_{2I}(p_1^3 - 3p_1q_1^2), \end{aligned} \tag{37}$$

where

$$\vartheta_1 = (2\sigma_1 + \sigma_2)/6, \quad \vartheta_2 = \sigma_2/2. \tag{38}$$

4.2. Combination parametric resonance

Following similar lines as in the previous case, we use the polar transformation for the complex amplitude A_n and arrive at the *reduced* equations for the modulation of amplitude and phase,

$$\begin{aligned} a_1' = {} & -\mu C_{1R}a_1 - \alpha e_{1R}a_1 - S_{1R}a_1^3 - S_{2R}a_1a_2^2 - G_{1R}a_1^2a_2\cos\gamma_1 + G_{1I}a_1^2a_2\sin\gamma_1 \\ & - H_{4R}a_2\cos(\gamma_2 - \gamma_1) + H_{4I}a_2\sin(\gamma_2 - \gamma_1), \end{aligned} \tag{39}$$

$$a_2' = -\mu C_{2R}a_2 - \alpha e_{2R}a_2 - S_{4R}a_2^3 - S_{3R}a_1^2a_2 - G_{2R}a_1^3\cos\gamma_1 - G_{2I}a_1^3\sin\gamma_1 - H_{5R}a_1\cos(\gamma_2-\gamma_1) + H_{5I}a_1\sin(\gamma_2-\gamma_1), \tag{40}$$

$$\gamma_1' = \sigma_1 + 3\mu C_{1I} + 3\alpha e_{1I} + 3S_{1I}a_1^2 + 3S_{2I}a_2^2 + 3G_{1R}a_1a_2\sin\gamma_1 + 3G_{1I}a_1a_2\cos\gamma_1 - \mu C_{2I} - \alpha e_{2I} - S_{4I}a_2^2 - S_{3I}a_1^2 + G_{2R}\frac{a_1^3}{a_2}\sin\gamma_1 - G_{2I}\frac{a_1^3}{a_2}\cos\gamma_1 + 3H_{4R}\frac{a_2}{a_1}\sin(\gamma_2-\gamma_1) + 3H_{4I}\frac{a_2}{a_1}\cos(\gamma_2-\gamma_1) - H_{5R}\frac{a_1}{a_2}\sin(\gamma_2-\gamma_1) - H_{5R}\frac{a_1}{a_2}\sin(\gamma_2-\gamma_1), \tag{41}$$

$$\gamma_2' = \sigma_1+\sigma_2 + 4\mu C_{1I} + 4\alpha e_{1I} + 4S_{1I}a_1^2 + 4S_{2I}a_2^2 + 4H_{4R}\frac{a_2}{a_1}\sin(\gamma_2-\gamma_1) + 4H_{4I}\frac{a_2}{a_1}\cos(\gamma_2-\gamma_1) + 4G_{1R}a_1a_2\sin\gamma_1 + 4G_{1I}a_1a_2\cos\gamma_1, \tag{42}$$

where $\gamma_1 = \beta_2 - 3\beta_1 + \sigma_1 T_1$ and $\gamma_2 = (\sigma_1+\sigma_2)T_1 - 4\beta_1$. The prime indicates the differentiation with respect to the slow time T_1. $S_{iR}, S_{iI}, H_{iR}, H_{iI}, G_{iR}, G_{iI}, C_{iR}, C_{iI}, e_{iI}, e_{iR}$ are the real and imaginary parts of the nonlinear interaction coefficients shown in the Appendix.

Due to the difficulty encountered for the stability analysis of the trivial state as indicated earlier, Cartesian formulation of the modulation equation is utilized instead, which leads to the *normalized reduced* equations

$$p_1' = -\mu C_{1R}p_1 - \mu C_{1I}q_1 - \alpha e_{1R}p_1 - \alpha e_{1I}q_1 - S_{1R}(p_1^3+p_1q_1^2) - S_{1I}(p_1^2q_1+q_1^3) - S_{2R}(p_1p_2^2+p_1q_2^2) - S_{2I}(q_1p_2^2+q_1q_2^2) - \vartheta_1 q_1 - H_{4R}p_2 + H_{4I}q_2 - G_{1R}(p_1^2p_2 - p_2q_1^2 + 2p_1q_1q_2) + G_{1I}(2p_1q_1p_2 - p_1^2q_2 + q_1^2q_2), \tag{43}$$

$$q_1' = -\mu C_{1R}q_1 + \mu C_{1I}p_1 - \alpha e_{1R}q_1 + \alpha e_{1I}p_1 + S_{1I}(p_1^3+p_1q_1^2) - S_{1R}(p_1^2q_1+q_1^3) - S_{2R}(q_1p_2^2+q_1q_2^2) + S_{2I}(p_1p_2^2+p_1q_2^2) + \vartheta_1 p_1 + H_{4R}q_2 + H_{4I}p_2 + G_{1R}(2p_1q_1p_2 - p_1^2q_2 + q_1^2q_2) + G_{1I}(p_1^2p_2 - p_2q_1^2 + 2p_1q_1q_2), \tag{44}$$

$$p_2' = -\mu C_{2R}p_2 - \mu C_{2I}q_2 - \alpha e_{2R}p_2 - \alpha e_{2I}q_2 - S_{4R}(p_2^3+p_2q_2^2) - S_{4I}(q_2^3+p_2^2q_2) - S_{3R}(p_1^2p_2+p_2q_1^2) - S_{3I}(p_1^2q_2+q_1^2q_2) - \vartheta_2 q_2 - H_{5R}p_1 + H_{5I}q_1 - G_{2R}(p_1^3 - 3p_1q_1^2) + G_{2I}(q_1^3 - 3p_1^2q_1), \tag{45}$$

$$q_2' = -\mu C_{2R}q_2 + \mu C_{2I}p_2 - \alpha e_{2R}q_2 + \alpha e_{2I}p_2 - S_{4R}(q_2^3+p_2^2q_2) + S_{4I}(p_2^3+p_2q_2^2) - S_{3R}(p_1^2q_2+q_1^2q_2) + S_{3I}(p_1^2p_2+p_2q_1^2) + \vartheta_2 p_2 + H_{6R}q_2 + H_{6I}p_2 + G_{2R}(q_1^3 - 3p_1^2q_1) + G_{2I}(p_1^3 - 3p_1q_1^2), \tag{46}$$

where

$$\vartheta_1 = (\sigma_1+\sigma_2)/4, \quad \vartheta_2 = (3\sigma_2-\sigma_1)/4. \tag{47}$$

For evaluating stability, the above equations are perturbed leading to

$$\{\Delta p_1', \Delta q_1', \Delta p_2', \Delta q_2'\}^{\mathrm{T}} = [J_c]\{\Delta p_1, \Delta q_1, \Delta p_2, \Delta q_2\}^{\mathrm{T}}. \tag{48}$$

The eigenvalues of the Jacobian matrix $[J_c]$ determine the stability and bifurcation of the system. The stability boundary for the trivial state is determined from the eigenvalues of the Jacobian matrix $[J_c]$ by setting $p_1 = q_1 = p_2 = q_2 = 0$.

5. Results and discussion

From the numerical computations it is found that the natural frequencies for different modes of the hinged–hinged pipe conveying fluid vary with the mean flow- velocity for specific values of other system parameters like fluid-pipe mass ratio, initial tension, dimensions and flexural stiffness of the pipe. The velocities corresponding to zero frequencies are the critical velocity of divergence or buckling. The natural frequencies for different modes are evaluated as functions of the fluid velocity u_0 corresponding to specific values of different system parameters. Taking the fluid-pipe mass ratio, $\beta = 0.64$ and initial tension parameter, $\Gamma = 25$, it is found that for the nondimensional mean flow velocity $u_0 = 2.773$, the natural frequency of the second mode is approximately equal to three times that of the first mode ($\omega_2 \approx 3\omega_1$) indicating the presence of 3:1 internal resonance. For these values of parameters, no other commensurable frequency relationships are observed, which obviates the possibility of nonlinear modal interaction among modes other than the first two. We study two cases of parametric resonance viz. principal parametric resonance of second mode, ($\Omega \approx 2\omega_2$) and combination parametric resonance of sum type ($\Omega \approx \omega_1 + \omega_2$) in presence of 3:1 internal resonance in the subcritical flow-velocity regime.

5.1. Principal parametric resonance

For the analysis of the pipe-fluid system subjected to principal parametric resonance of the second mode (i.e., $\Omega \approx 2\omega_2$) in presence of 3:1 internal resonance, system parameters are taken as mentioned earlier corresponding to the commensurable natural frequencies of the first and second mode of the system and $k = 9050$ for the nonlinearity parameter. There are no modal interactions involving other modes. The specific value of the flow velocity used for the study, considering internal frequency detuning, is $u_0 = 3.0$ for which $\omega_1 = 15.337$ and $\omega_2 = 46.945$. The book-keeping parameter ε is taken as 0.01. The corresponding internal detuning parameter $\sigma_1 = 93.4$.

The trivial state stability boundary is shown in Fig. 2, plotted in terms of parametric frequency detuning σ_2 for the chosen parameter values and for different values of the damping. The region inside the boundary denotes instability. In the absence of internal resonance, the present problem reduces to that of Namachchivaya [9]. Corresponding to typical values of system parameters used in Ref. [9] for a horizontal pipe without initial tension, viz $u_0 = 1.88$, $\beta = 0.64$, $\alpha^* = 0.005$, $\Gamma = 0$, $\omega_{01} = 9.87$ (the dimensionless natural frequency in the first mode at zero flow velocity), $\omega_1 = 7.71$, $\omega_2 = 38.55$ and $\Omega \approx 2\omega_2$ (principal parametric resonance), the results for the stability boundaries are found to be in good agreement.

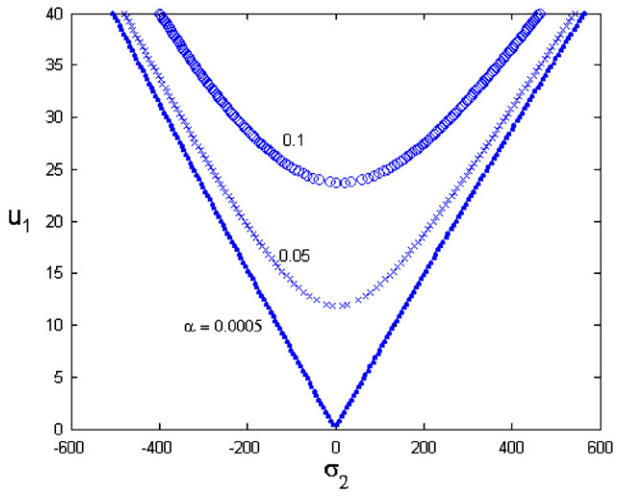

Fig. 2. Trivial state stability boundary for different values of damping parameter. Values of the nondimensional damping parameter α indicated on the curves.

5.1.1. Stability and bifurcations of equilibrium solutions

The nonlinear steady-state response along with their stability and bifurcations are obtained by utilizing the reduced equations or normalized reduced equations representing the modulations in the system response. Frequency and amplitude response curves are found to be symmetrical about the σ_2 and u_1 axes respectively and hence only the positive sides of the response curves are presented here. The normal continuous lines in the figure represent stable equilibrium solutions, the bold lines the unstable foci and the dotted lines the saddle.

Typical frequency response curves for the first and second modes are shown in Fig. 3 for $\mu = 0.1$, $u_1 = 10$ and $\sigma_1 = 93.4$. The response curves in this case have trivial, single-mode and two-mode equilibrium solutions. Two-mode equilibrium solutions are found for specific range of parameter values and are isolated from the single-mode solutions. The single-mode solutions show a hardening-spring-type behavior. The nontrivial single- mode response a_2 has a stable branch and an unstable branch having supercritical and subcritical pitchfork bifurcations from the trivial state at $\sigma_2 = -132.796$ and $\sigma_2 = 131.39$ respectively. The isolated two-mode solutions are in the form of closed loops and have stable portion between the limit point SN_2 ($\sigma_2 = 340.53$) and the Hopf bifurcation point H_1 ($\sigma_2 = 326.49$). Fig. 4 shows the frequency response curve

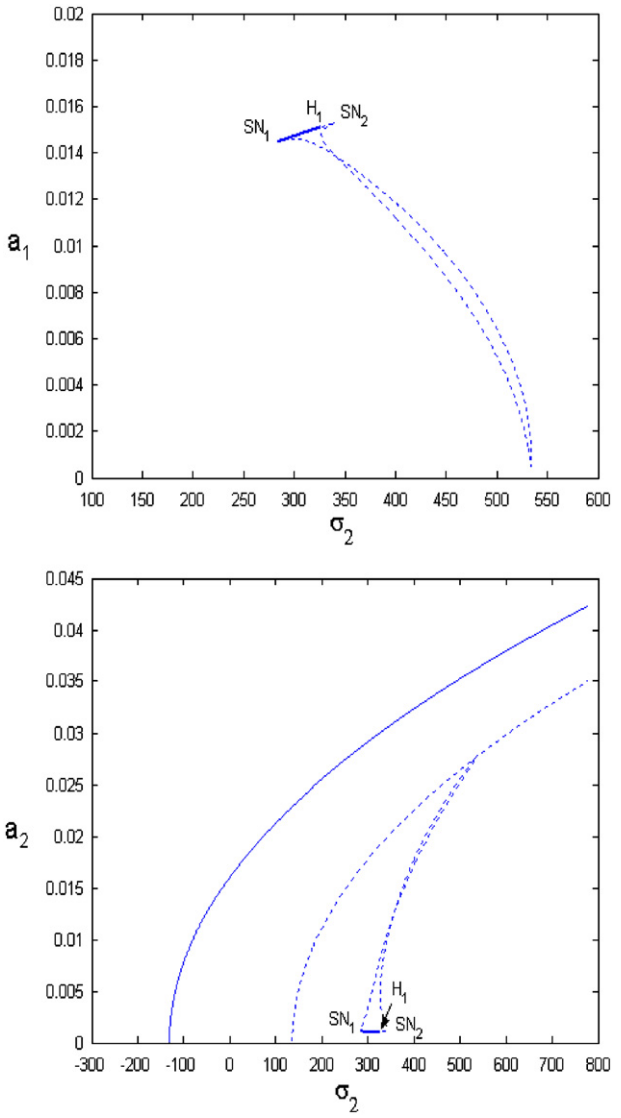

Fig. 3. Frequency response curve for $\mu = 0.1$, $\alpha = 0$, $u_1 = 10$ and $\sigma_1 = 93.4$.

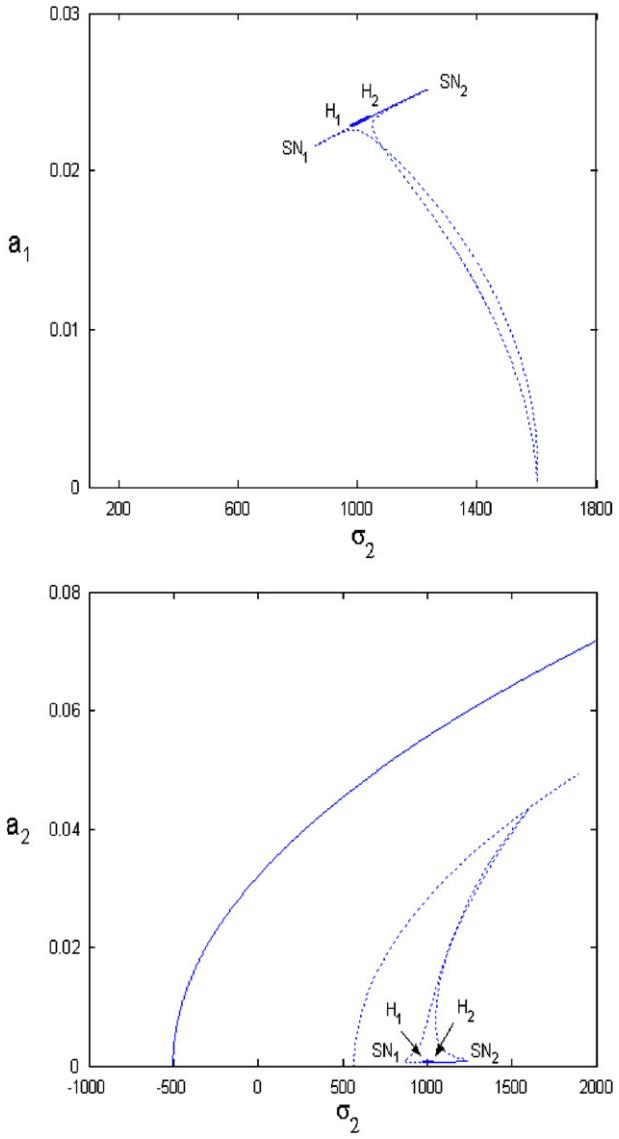

Fig. 4. Frequency response curve for $\mu = 0.1$, $\alpha = 0$, $u_1 = 40$ and $\sigma_1 = 93.4$.

corresponding to higher amplitude of flow-velocity-fluctuation for $\mu = 0.1$, $u_1 = 40$ and $\sigma_1 = 93.4$. It follows that for higher magnitude of flow-pulsation, the range between the stable and unstable branches of the single-mode solution widens and the loops of the two-mode solution broaden indicating increase in the strength of the nonlinear modal interaction.

The effect of internal frequency detuning parameter (σ_1) on the frequency response is shown in Figs. 5 and 6 for specific values of amplitude ($u_1 = 10$) of flow-pulsation. It follows that for lower values of σ_1, the strength of the nonlinear interaction due to the three-to-one internal resonance weakens, the amplitudes of both modes decrease, which is more pronounced for the indirectly excited first mode. For the single-mode (second mode) response, the separation of the nontrivial stable and unstable curve decreases with decreasing σ_1.

Fig. 7 shows typical amplitude-response curves for $\sigma_1 = 93.4$ and $\sigma_2 = 330$. As in the case of the frequency response, the amplitude response also has single-mode and two-mode solutions besides the trivial solution.

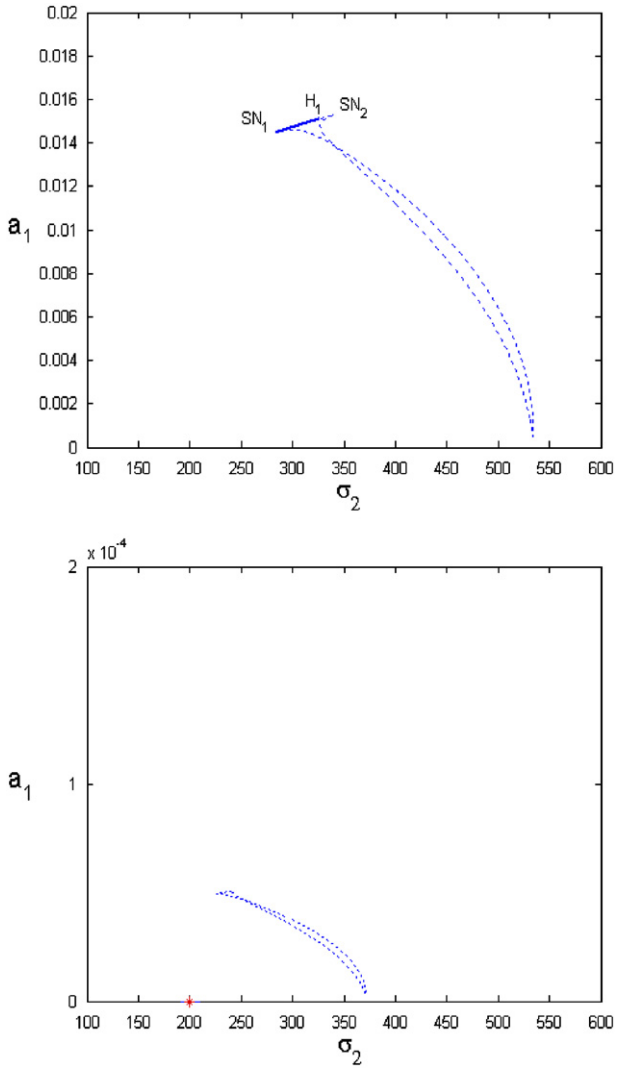

Fig. 5. Frequency response curves (first mode) for $\mu = 0.1$, $\alpha = 0$, $u_1 = 10$ and (a) $\sigma_1 = 93.4$, (b) $\sigma_1 = 18.43$.

With increase in the amplitude of flow-pulsation u_1, the trivial state of the second mode loses stability at $u_1 = 23.9$ through a subcritical pitchfork bifurcation resulting in a jump of the response to the stable nontrivial branch which shows a monotonic increase with u_1. The isolated two- mode solutions in the form of closed loops exist in specific range of the flow-pulsation amplitude u_1 and have stable portion between the limit points SN_1 ($u_1 = 9.569$) and the Hopf bifurcation point H_1 ($u_1 = 10.16$).

If we do not consider the internal resonance and flexural rigidity in the system, the present problem reduces to that of the pipe conveying fluid studied by Oz [22]. The frequency response curves for the case of principal parametric resonance in both the studies (i.e., in Ref. [22] and the present one) are in qualitative agreement displaying trivial and single mode nontrivial solutions along with pitchfork bifurcations. In a similar study of the axially moving beam [23], which belongs to the broader class of traveling continua like pipes conveying fluid and also in the study of pipes conveying fluid by Namachchivaya [9], this qualitative feature is also displayed in absence of internal resonance. In contrast, the additional two mode solutions in the form of closed loops for the frequency response curves and amplitude response curves are observed in the present problem, which are the contributions of internal resonance.

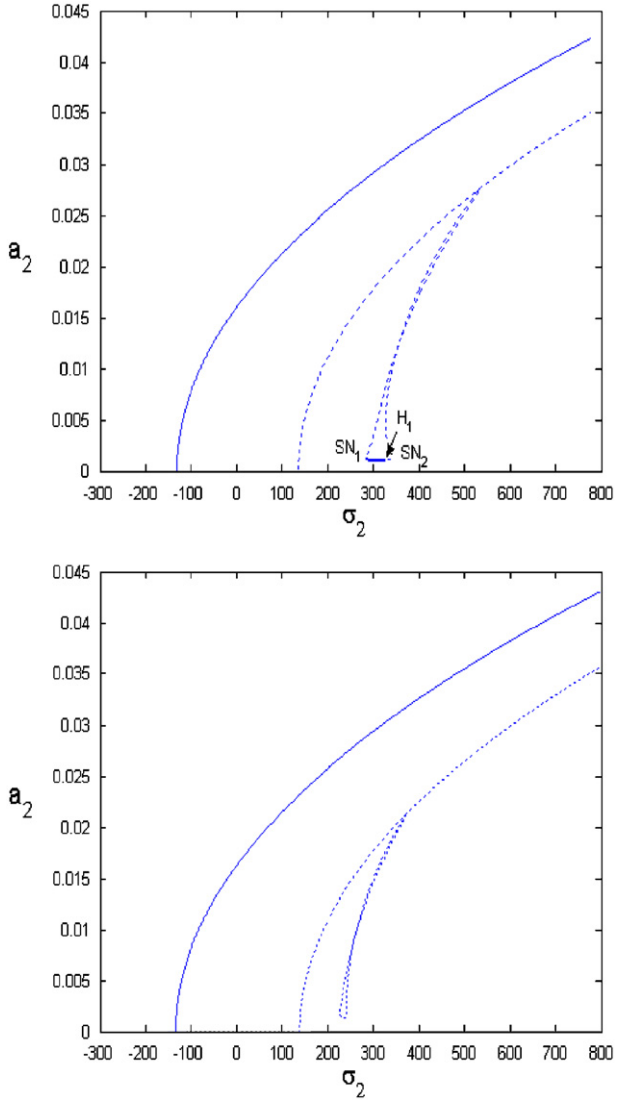

Fig. 6. Frequency response curve (second mode) for $\mu = 0.1$, $\alpha = 0$, $u_1 = 10$ and (a) $\sigma_1 = 93.4$, (b) $\sigma_1 = 18.43$.

5.1.2. Dynamic solutions

Some typical dynamic solutions are presented corresponding to the frequency response and amplitude response plots. Taking initial conditions in the vicinity of the nontrivial single-mode equilibrium solutions (Fig. 4), the system has periodic response in the second mode as shown in the form of phase portrait, FFT power spectra and Poincare maps, typically at $\sigma_2 = 400.05$, $\mu = 0.1$, $\alpha = 0$ and $u_1 = 40$ (Fig. 8). The first mode response attains trivial state. The system exhibits quasiperiodic behaviour in the second mode for another value of the detuning parameter, i.e., at $\sigma_2 = 150.75$, $\mu = 0.1$, $\alpha = 0$ and $u_1 = 40$ as indicated in Fig. 9 in the form of time history and Poincare maps. The first mode response goes to trivial state. The quasiperiodic nature of the second mode is apparent from the beating effect of the time response and closed loop feature of the Poincare map. Fig. 10 shows the trivial state in the first mode and quasiperiodic response in the second mode corresponding to another point of the frequency response plot, viz. at $\sigma_2 = 700.05$, $\mu = 0.1$, $\alpha = 0$ and $u_1 = 40$. In the stable portion of the closed loop frequency response curves, for typical detuning parameter $\sigma_2 = 1230.1$, $\mu = 0.1$, $\alpha = 0$ and $u_1 = 40$, the two-mode system response is shown in Fig. 11. While the first mode jumps to the trivial state, the second mode exhibits periodic behaviour. These sample dynamic solutions indicate periodic, quasiperiodic and mixed mode response of the system for the chosen parameter values.

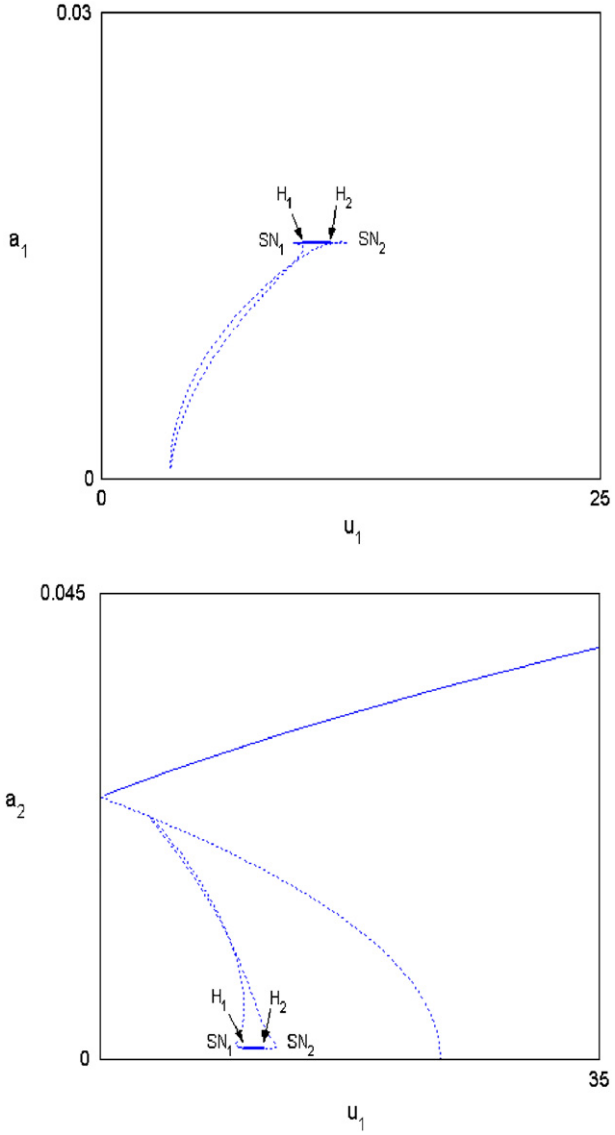

Fig. 7. Amplitude response curves for $\mu = 0.1$, $\alpha = 0$, $\sigma_2 = 330$.

5.2. Combination parametric resonance

For analysis of the pipe-fluid system subjected to combination parametric resonance of the additive type ($\Omega \approx \omega_1 + \omega_2$) in presence of 3:1 internal resonance, the system parameters like mass ratio, tension parameter, nonlinearity parameter and flow velocity are taken same as in the previous case, which corresponds to similar natural frequencies and internal frequency detuning parameter as stated earlier. The trivial state stability boundary is shown in Fig. 12, plotted in terms of parametric frequency detuning σ_2, for different values of the damping parameter. In the absence of internal resonance, the present problem reduces to that of Namachchivaya [10]. Corresponding to typical values of system parameters used in Ref. [10] for a horizontal pipe without initial tension, viz $u_0 = 1.88$, $\beta = 0.64$, $\alpha^* = 0.005$, $\Gamma = 0$, $\omega_{01} = 9.87$ (the dimensionless natural frequency in the first mode at zero flow velocity), $\omega_1 = 7.71$, $\omega_2 = 38.55$ and $\Omega \approx \omega_1 + \omega_2$ (combination parametric resonance), the results for the stability boundaries are found to be in good agreement.

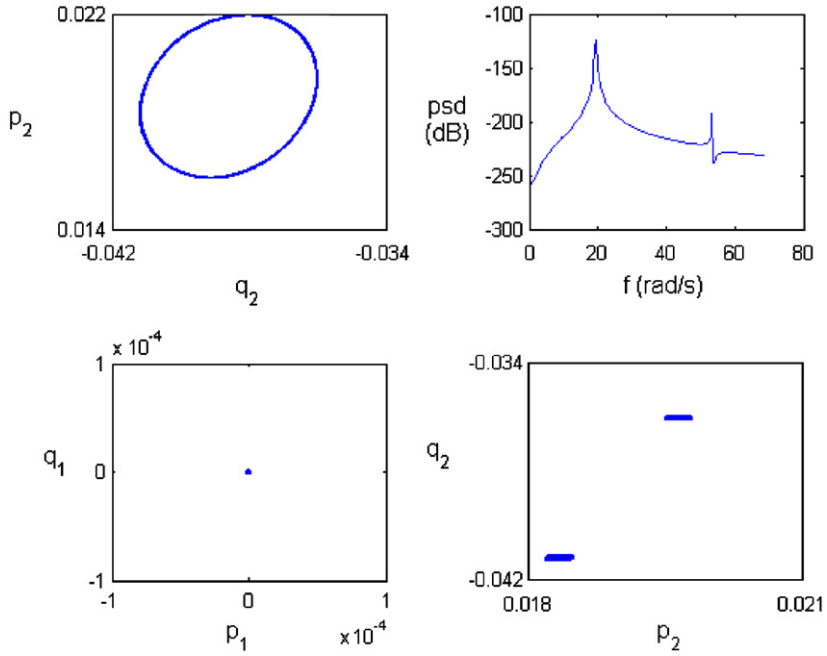

Fig. 8. Phase portrait, FFT power spectra and Poincare map for $\sigma_2 = 400.05$, $\mu = 0.1$, $\alpha = 0$, $u_1 = 40$.

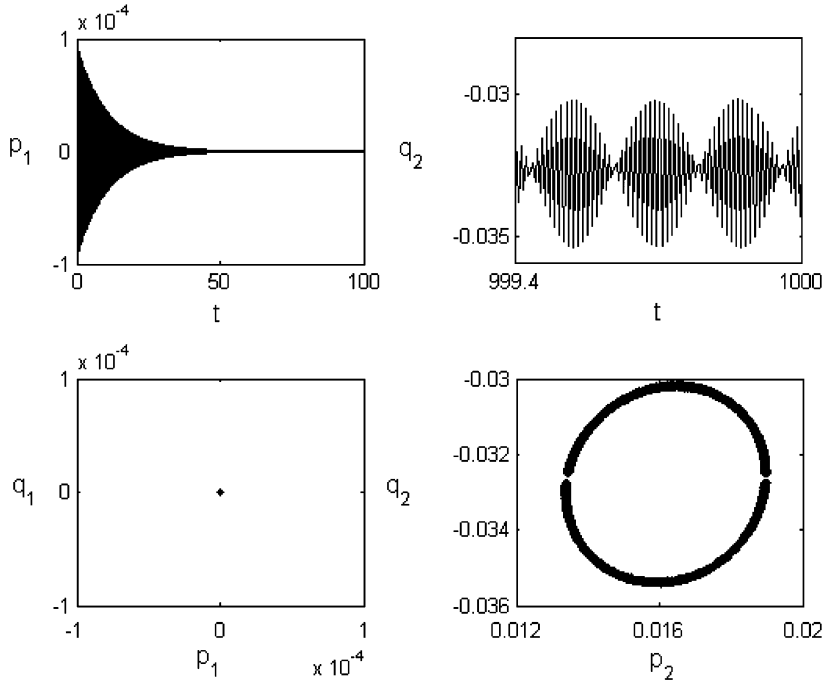

Fig. 9. Time history and Poincare map for $\sigma_2 = 150.75$, $\mu = 0.1$, $\alpha = 0$ and $u_1 = 40$.

5.2.1. Stability and bifurcations of equilibrium solutions

As in the case of principal parametric resonance, the frequency and amplitude response curves for the first and second modes are found to be symmetrical about the σ_2 and u_1 axes respectively and hence only the

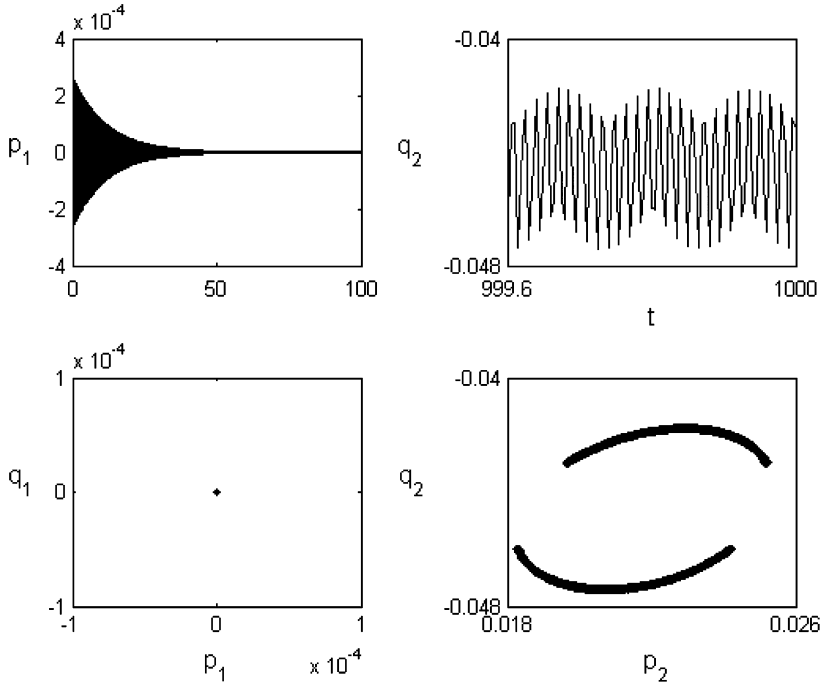

Fig. 10. Time history and Poincare map for $\sigma_2 = 700.05$, $\mu = 0.1$, $\alpha = 0$ and $u_1 = 40$.

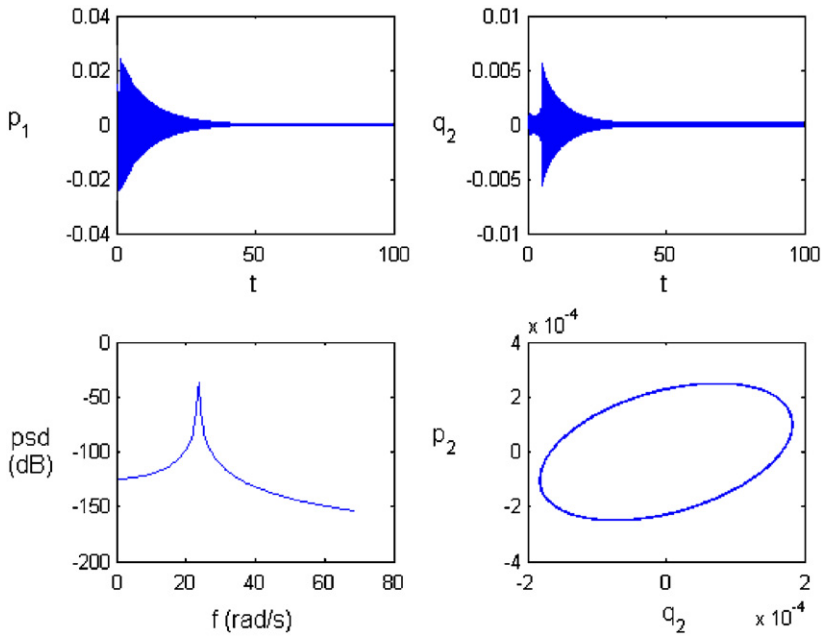

Fig. 11. Time history, FFT power spectra and phase portrait for $\sigma_2 = 1230.1$, $\mu = 0.1$, $\alpha = 0$ and $u_1 = 40$.

positive sides of the response curves are presented here. Typical frequency response curves for the first and second mode are shown in Fig. 13 for $\mu = 0.1$, $u_1 = 6$ and $\sigma_1 = 93.4$. The system exhibits isolated two-mode nontrivial equilibrium solutions coexisting with the trivial solution. One of these isolated nontrivial solutions

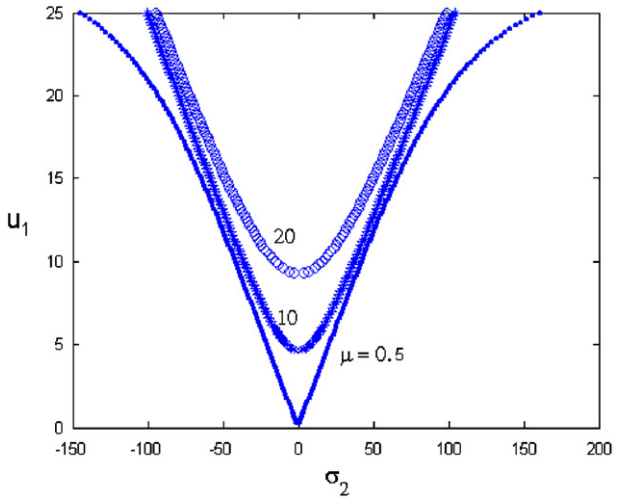

Fig. 12. Trivial state stability boundary for different values of damping parameter.

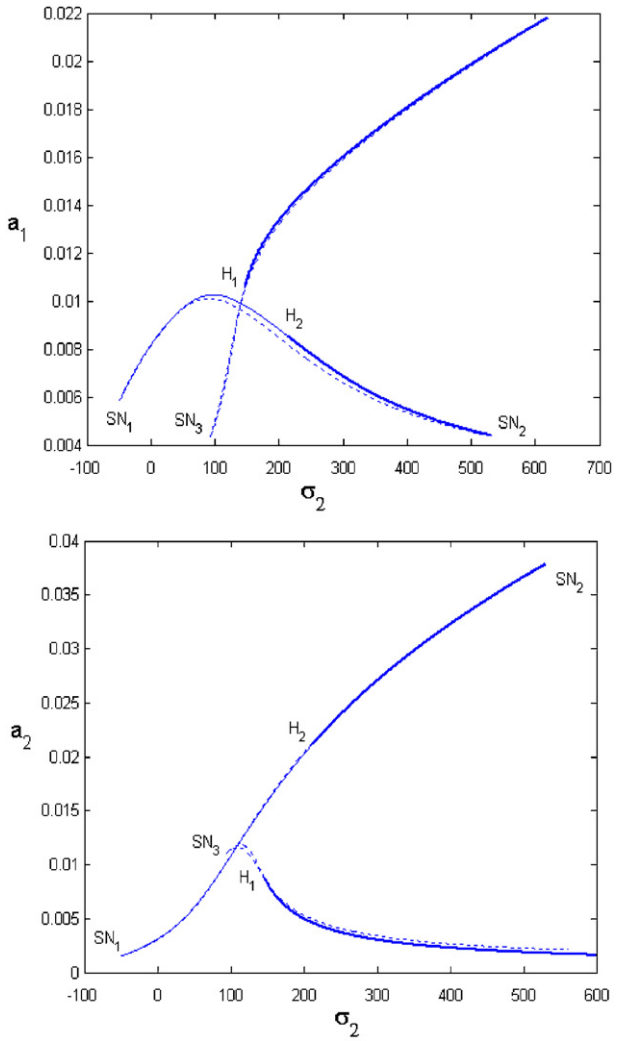

Fig. 13. Frequency response curves for $\mu = 0.1$, $\alpha = 0$, $u_1 = 6$ and $\sigma_1 = 93.4$.

is in the form of a closed loop lying between two limit points at SN_1 ($\sigma_2 = -49.1834$) and SN_2 ($\sigma_2 = 530.5504$). The upper branch has a Hopf bifurcation at H_2 ($\sigma_2 = 212.4658$), where one pair of complex conjugate eigenvalues crosses the imaginary axis from the left-half of the complex plane to the right-half leading to instability. The other isolated nontrivial portion of the equilibrium solution has a limit point at SN_3 ($\sigma_2 = 92.156$) where the response jumps to one of the two other branches of stable equilibrium solutions, one trivial and another nontrivial solution of the closed loop, depending on the initial conditions. This isolated nontrivial solution continues for higher values of the detuning parameter σ_2 as a pair of branches. With increase in σ_2, the amplitude of first mode increases steadily along these nontrivial branches, while the second mode amplitude decreases continuously. The upper nontrivial branch has a Hopf bifurcation at point H_1 ($\sigma_2 = 146.416$). The trivial state is stable throughout the range of detuning parameter σ_2 except in the zone between the Hopf bifurcation points at $\sigma_2 = -25.562$ and $\sigma_2 = 25.802$. Fig. 14 shows frequency response curves for higher value of amplitude of flow-pulsation typically for $\mu = 0.1$, $u_1 = 18$ and $\sigma_1 = 93.4$. With increase in flow-pulsation, the range of the nontrivial closed loop diminishes and additional Hopf bifurcation point appears.

Fig. 15 shows the variation of amplitude of response for the first and the second mode with the amplitude of flow-pulsation u_1, for $\mu = 0.1$, $\alpha = 0$, $\sigma_2 = 120$ and $\sigma_1 = 93.4$. As in the case of the frequency response, the amplitude response also has two portions of isolated nontrivial curves, one a closed loop and another continuously varying with increasing detuning parameter. The closed-loop portion of the nontrivial state

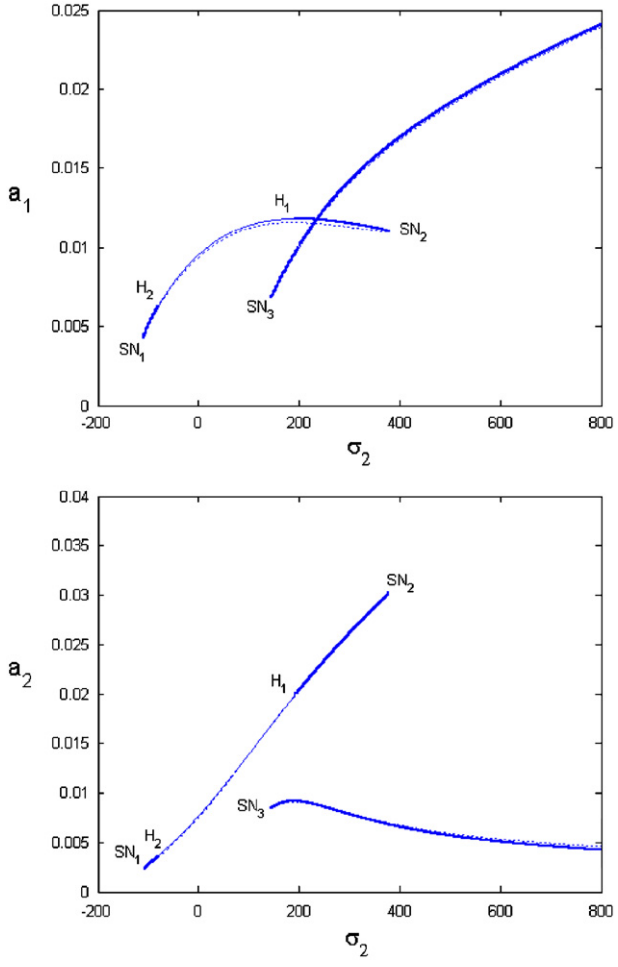

Fig. 14. Frequency response curves for $\mu = 0.1$, $\alpha = 0$, $u_1 = 18$ and $\sigma_1 = 93.4$.

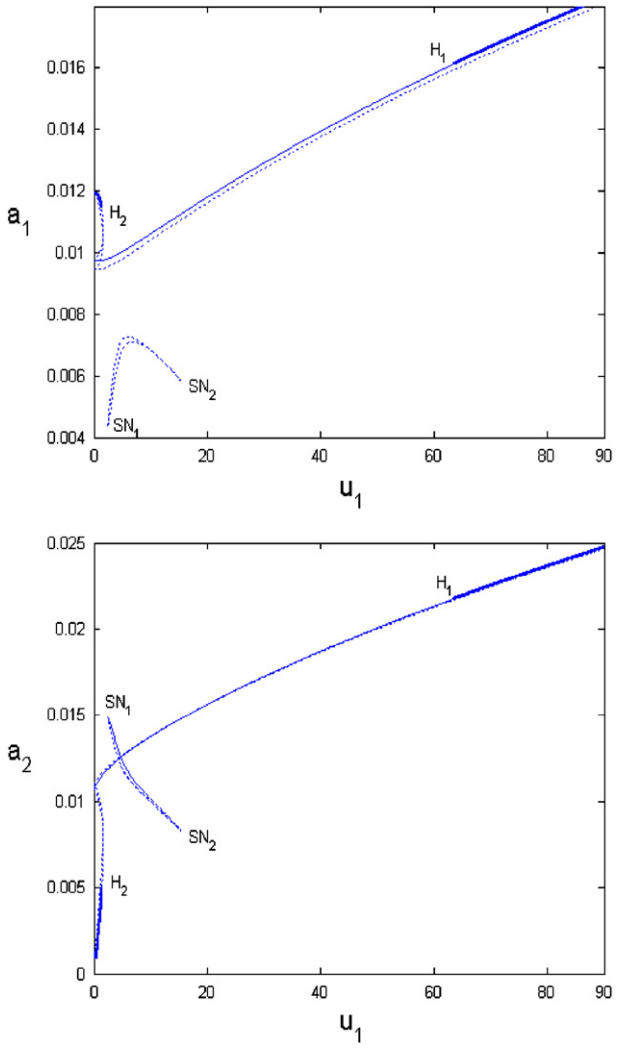

Fig. 15. Amplitude response curves for $\mu = 0.1$, $\alpha = 0$, $\sigma_2 = 120$ and $\sigma_1 = 93.4$.

ranges between the limit points SN_1 ($\sigma_2 = 2.465$) and SN_2 ($\sigma_2 = 15.305$) and is unstable. In the second branch of the nontrivial solution, one branch is stable and continuously increasing for both the modes for increasing values of u_1. This branch has a Hopf bifurcation point H_1 ($\sigma_2 = 63.564$). For lower values of u_1, this stable branch loses stability through a succession of saddle-node bifurcations leading to the unstable branches, which has another Hopf bifurcation point at H_2 ($\sigma_2 = 1.427$). When the fluctuation amplitude u_1 increases from a low value, the stable equilibrium system response is either trivial or nontrivial depending on the initial conditions. With increase in u_1, amplitudes of both the modes increase monotonically.

5.2.2. Dynamic solutions

The frequency-response and amplitude-response plots show a number of bifurcations with variation of control parameters u_1 and σ_2 of flow-velocity-fluctuation. Dynamic behavior of the system in the form of periodic, quasiperiodic and chaotic responses is investigated in the vicinity of the bifurcation points and some sample results are presented. The response is dependent on the initial conditions. A variety of response behavior is observed. Near the Hopf bifurcation point H_2 in the unstable portion of the nontrivial closed loop in the frequency response curve (Fig. 13) corresponding to detuning parameter $\sigma_2 = 215.58$ and with $\mu = 0.1$, $u_1 = 6$ and $\sigma_1 = 93.4$, the system response jumps to the trivial state as shown in the time history and Poincare

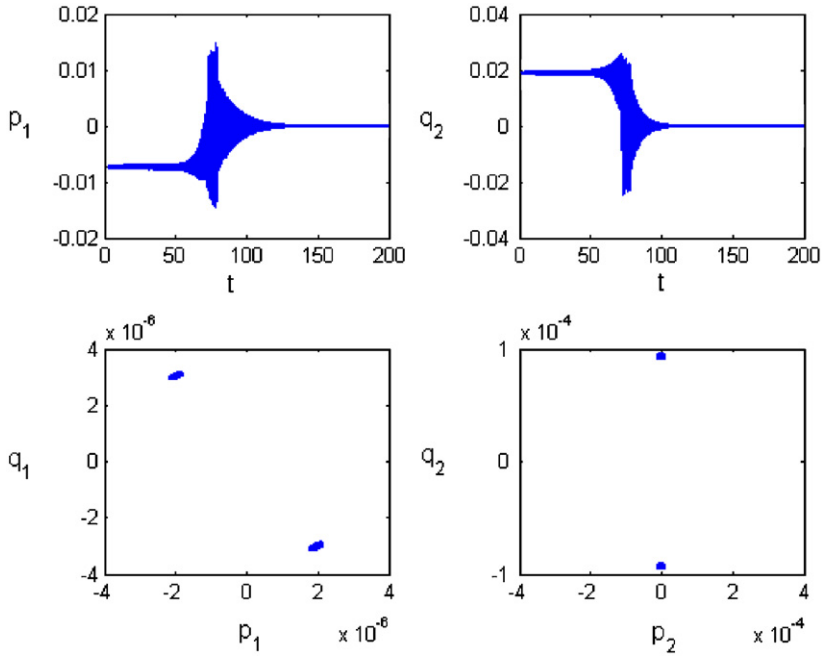

Fig. 16. Time history and Poincare map for $\sigma_2 = 215.58$, $\mu = 0.1$, $\alpha = 0$, $u_1 = 6$ and $\sigma_1 = 93.4$.

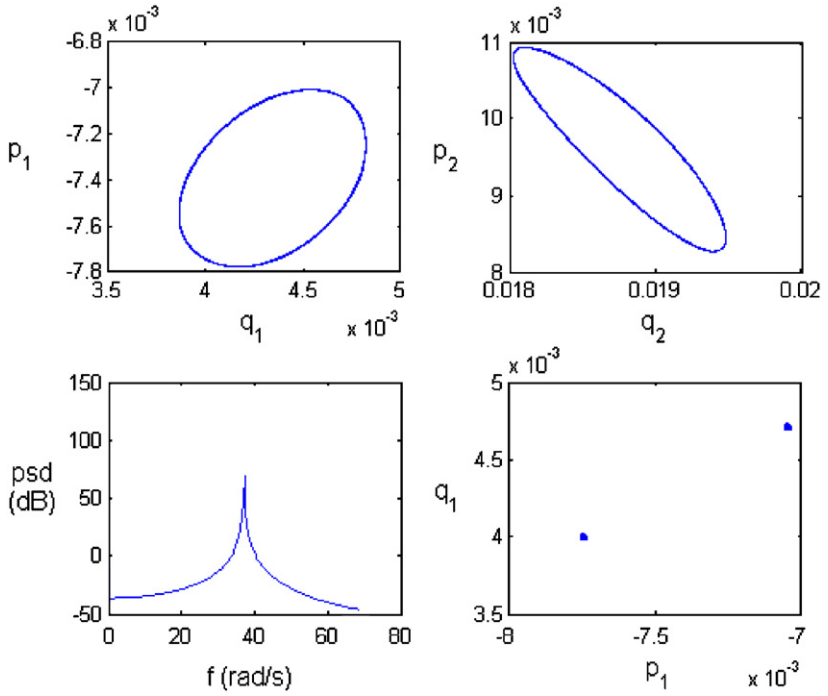

Fig. 17. Phase portrait, FFT power spectra and Poincare map for $\sigma_2 = 211.58$, $\mu = 0.1$, $\alpha = 0$, $u_1 = 6$ and $\sigma_1 = 93.4$.

map of Fig. 16. Corresponding to another nearby point on the same branch at $\sigma_2 = 211.58$, the system has periodic solutions as indicated in Fig. 17 in the form of phase portrait, FFT power spectra and Poincare map. For another point on this branch, closer to the crossing of the other isolated nontrivial unstable branch at

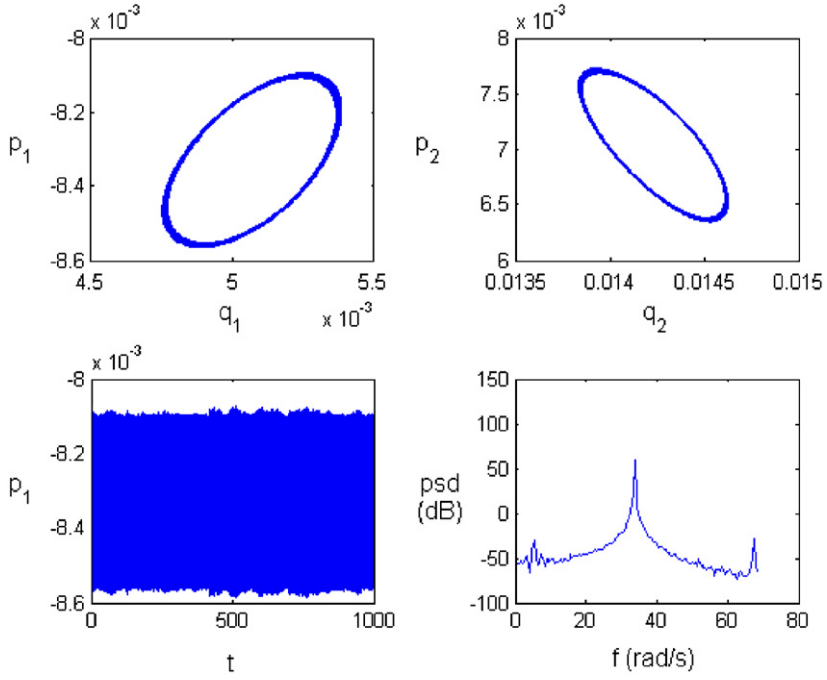

Fig. 18. Phase portrait, time history and power spectra for $\sigma_2 = 150.58$, $\mu = 0.1$, $\alpha = 0$, $u_1 = 6$ and $\sigma_1 = 93.4$.

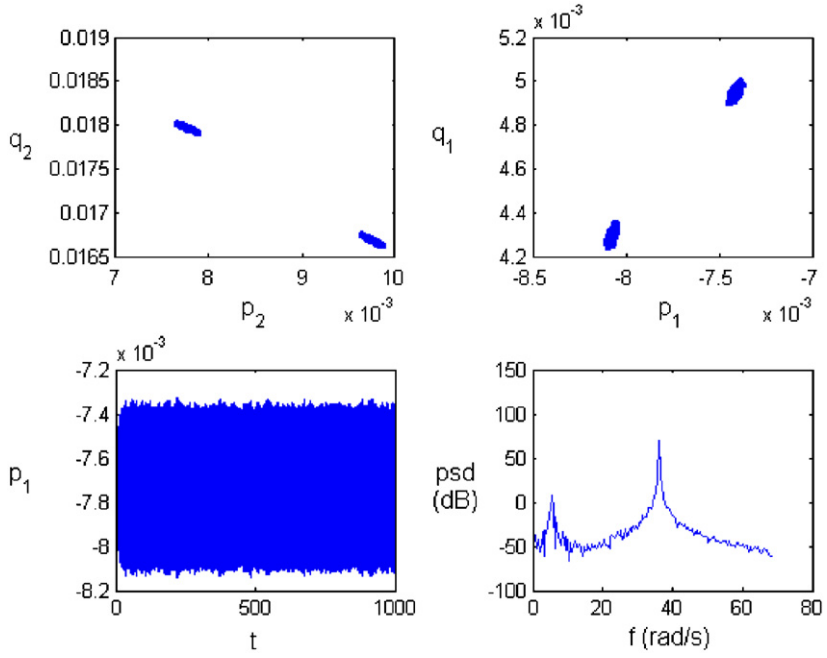

Fig. 19. Poincare map, time history and power spectra for $\sigma_2 = 190.58$, $\mu = 0.1$, $\alpha = 0$, $u_1 = 6$ and $\sigma_1 = 93.4$.

$\sigma_2 = 150.58$, the system exhibits motion with mild chaotic modulation as depicted through phase portrait, time history and FFT power spectra in Fig. 18. The Poincare map, time history and FFT power spectra of Fig. 19 also correspond to chaotically modulated motion for another point $\sigma_2 = 190.58$ on this branch.

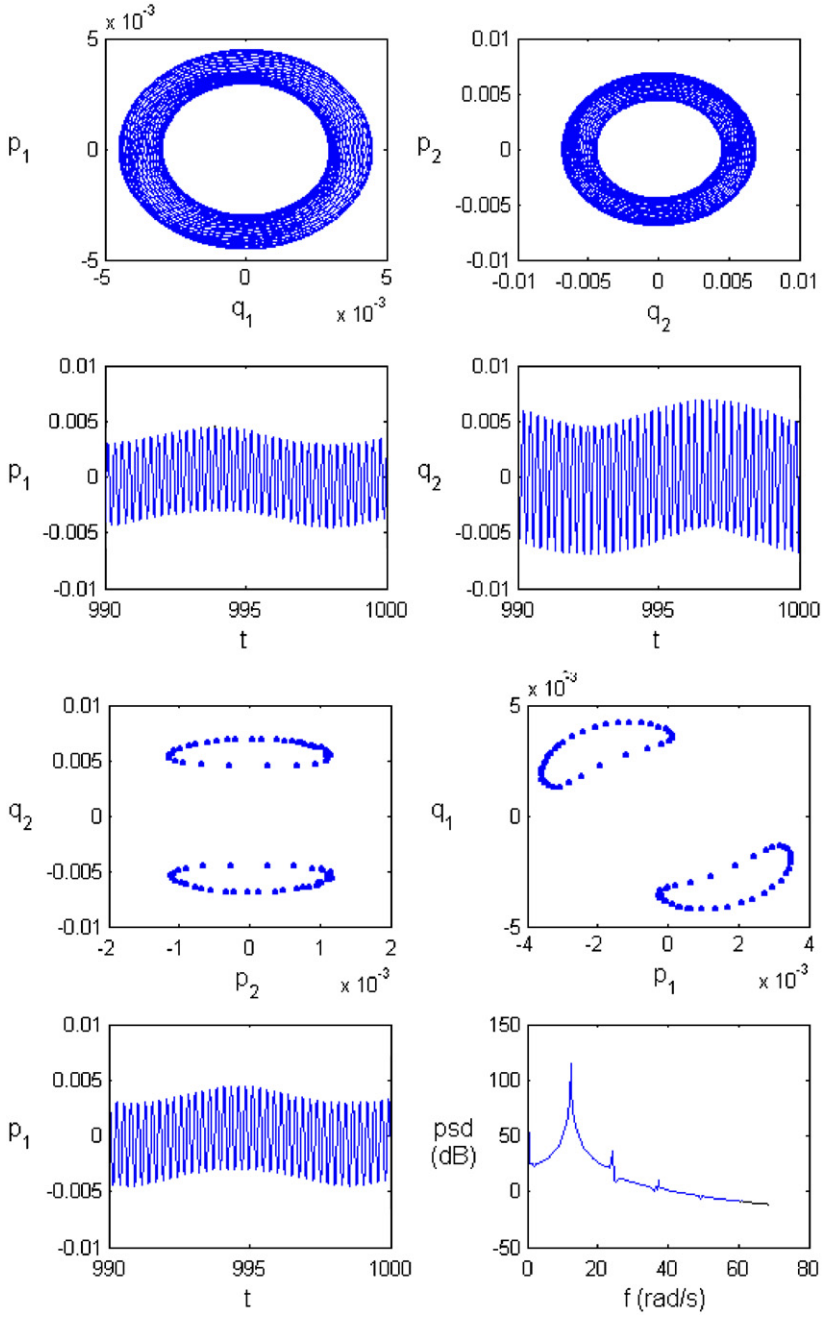

Fig. 20. Phase portrait, time history, Poincare map and power spectra for $\sigma_2 = 200.58$, $\mu = 0.1$, $\alpha = 0$, $u_1 = 6$ and $\sigma_1 = 93.4$.

For some range of the detuning parameters, the system exhibits a mix of quasiperiodic and transitional behavior. For example, at $\sigma_2 = 200.58$, the response is quasiperiodic as shown in Fig. 20. The torus form of the phase portrait, the beating effect in the time history and the closed loop form of the Poincare map indicate this quasiperiodic nature of response. The transitional behaviour in the form of torus breakdown is observed for $\sigma_2 = 210.58$, $\mu = 0.1$, $u_1 = 6$ and $\sigma_1 = 93.4$ (Fig. 21). The above results are for relatively lower value of flow pulsation. For higher magnitude of pulsation, system also exhibits a wide array of dynamical behaviour. Corresponding to the frequency response plot in Fig. 14, for $\mu = 0.1$, $u_1 = 18$ and $\sigma_1 = 93.4$ in the vicinity of

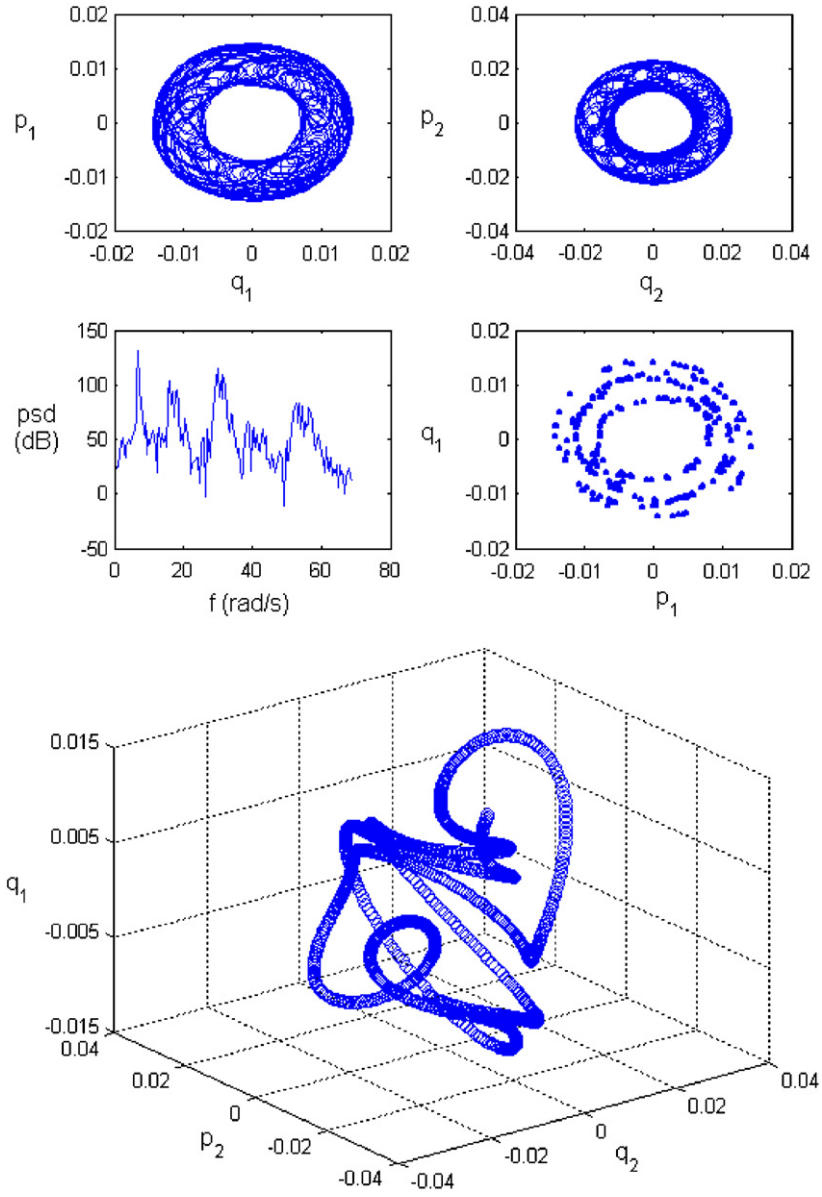

Fig. 21. Phase portrait, time history, Poincare map and power spectra for $\sigma_2 = 210.58$, $\mu = 0.1$, $\alpha = 0$, $u_1 = 6$ and $\sigma_1 = 93.4$.

the Hopf bifurcation point H_2 at $\sigma_2 = -81.488$ in the stable portion of the branch, the system response is shown in Fig. 22 through the phase portrait, time history and Poincare map. Torus form of the phase portrait, beating phenomena in time history and closed loop character of the Poincare map indicate quasiperiodic behaviopur. Fig. 23 shows the phase portrait and Poincare map for another nearby point in the same branch at $\sigma_2 = -80.419$. The response is also quasiperiodic in nature. For the portion of the branch corresponding to unstable foci in the vicinity of H_2, the response grows and jumps to the trivial attractor, about which the system executes periodic motion. Fig. 24 characterizes this feature for $\sigma_2 = -90.419$. A mix of quasiperiodic and transitional behaviour is observed for points in the range between Hopf bifurcation points H_1 and H_2 in the above branch. For example, at $\sigma_2 = 134.38$, the quasiperiodic response is shown through Poincare map, time history and power spectra in Fig. 25. The transitional behaviour with torus breakdown is depicted in the form of phase portrait, power spectra and Poincare map in Fig. 26 for another point at $\sigma_2 = 183.88$

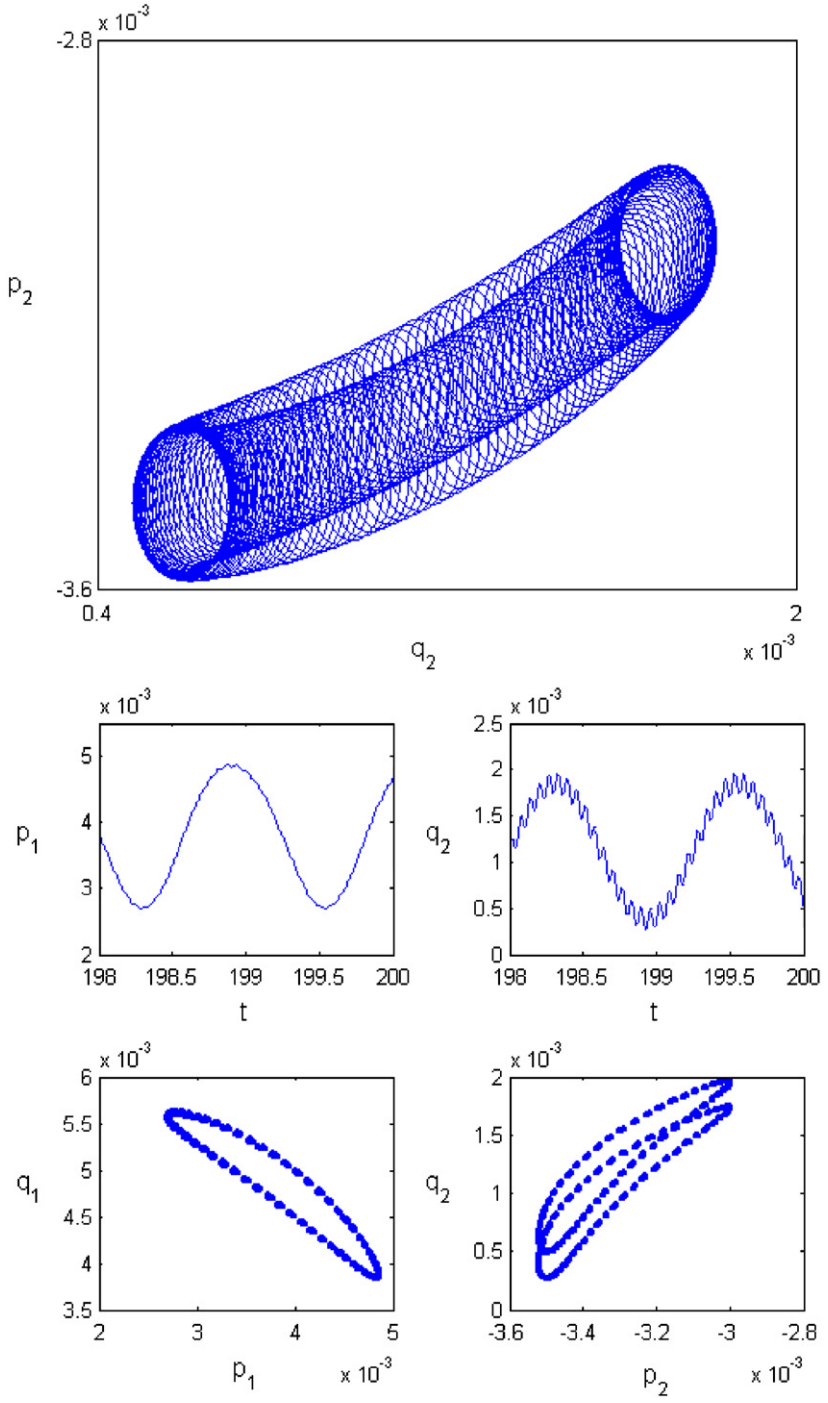

Fig. 22. Phase portrait, time history and Poincare map for $\sigma_2 = -81.488$, $\mu = 0.1$, $\alpha = 0$, $u_1 = 18$ and $\sigma_1 = 93.4$.

closer to H_1. For points closer to the limit point SN_2, the system exhibits chaotic behaviour as shown in the phase portrait, power spectra and Poincare map typically for $\sigma_2 = 341.72$ in Fig. 27. These are some illustrations of a wide range of behaviour displayed by the system under the combination parametric resonance and internal resonance.

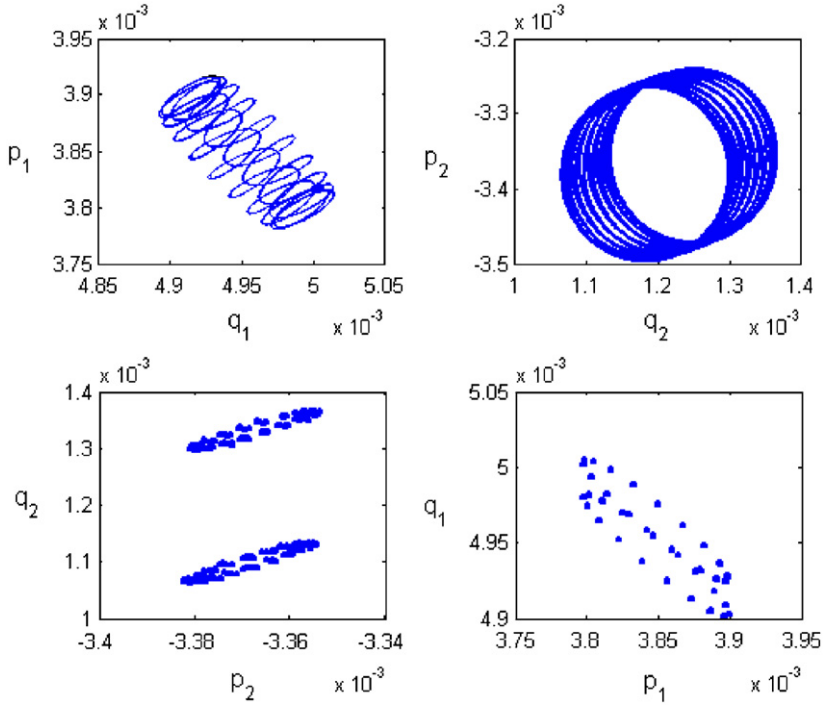

Fig. 23. Phase portrait and Poincare map for $\sigma_2 = -80.419$, $\mu = 0.1$, $\alpha = 0$, $u_1 = 18$ and $\sigma_1 = 93.4$.

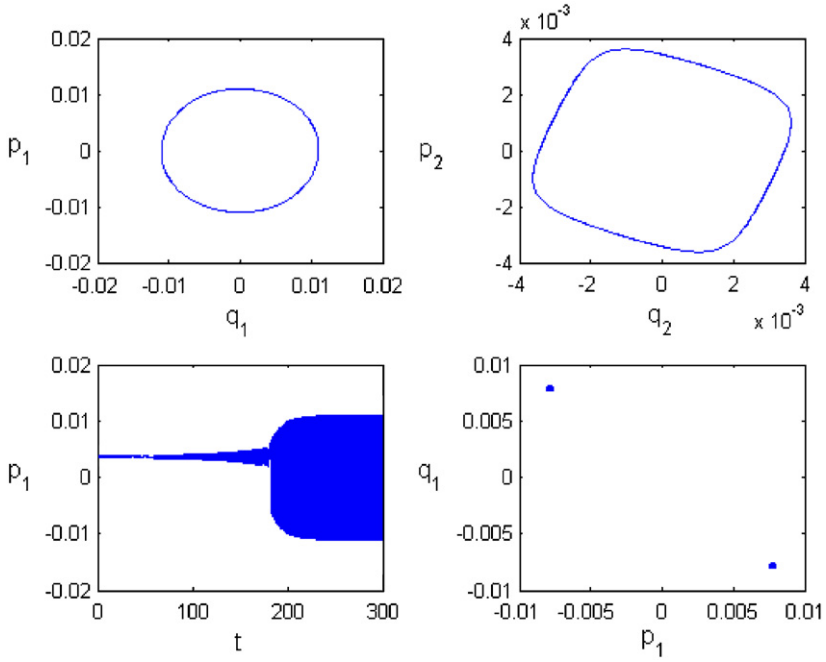

Fig. 24. Phase portrait, time history and Poincare map for $\sigma_2 = -90.419$, $\mu = 0.1$, $\alpha = 0$, $u_1 = 18$ and $\sigma_1 = 93.4$.

6. Conclusion

Though in conventional beams with hinged–hinged boundary conditions having classical mode shapes and stretching-related cubic nonlinearity internal resonance is not possible due to vanishing of the nonlinear

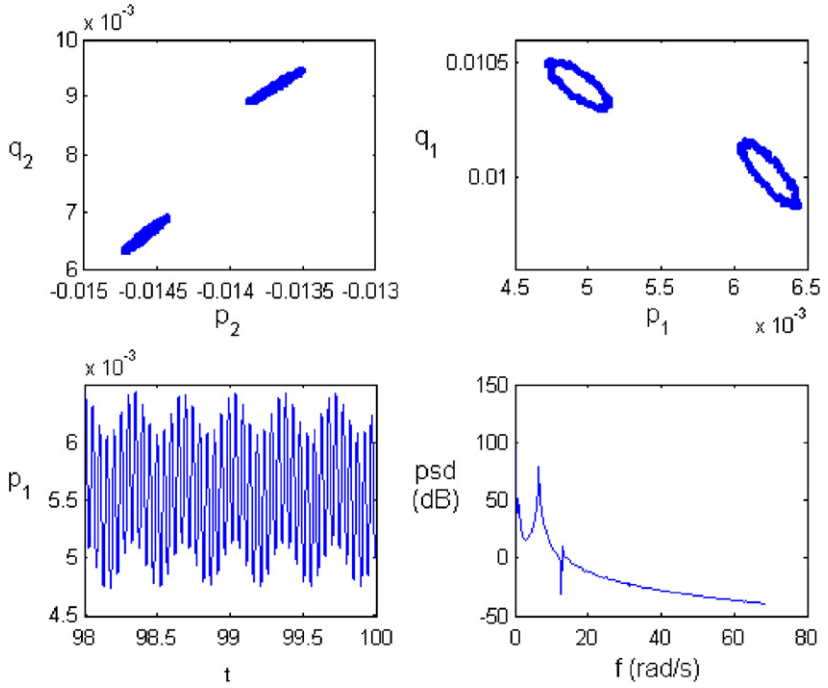

Fig. 25. Poincare map, time history and power spectra for $\sigma_2 = 134.38$, $\mu = 0.1$, $\alpha = 0$, $u_1 = 18$ and $\sigma_1 = 93.4$.

interaction coefficients, internal resonance is possible with consequent repercussions on the system behavior in case of pipes conveying fluid with similar boundary conditions and nonlinearity. As a result of nonlinear modal interactions involving two modes, responses in these directly and indirectly excited modes exist whereas those in other modes are damped out.

The nonlinear pipe conveying fluid with harmonic velocity pulsation can exhibit a wide array of dynamic behavior in presence of 3:1 internal resonance under principal parametric resonance of second mode and combination parametric resonance due to parametric excitation related to the flow pulsation. The internal resonance in pipes conveying fluid, which is not explored so far, is studied.

For the case of principal parametric resonance of second mode, single-mode solution and isolated two-mode solutions exist besides the trivial state in the frequency response and amplitude response. The two mode solutions are the contributions of internal resonance in the system. The frequency response curves corresponding to single-mode solutions exhibit a hardening spring-behavior. In the single mode response, nontrivial steady-state solutions bifurcate from the trivial solutions through supercritical and subcritical pitchfork bifurcations for the frequency response and through subcritical pitchfork bifurcation for the amplitude response. Besides the pitchfork bifurcations, the system undergoes Hopf bifurcations and saddle node bifurcations for variation of control parameters viz. frequency detuning and amplitude of pulsation.

Two mode equilibrium solutions exist for specific range of parameter values and are isolated from the single mode solutions. For higher magnitude of flow pulsation the strength of the nonlinear modal interaction increases. For lower values of the internal frequency detuning parameter, the strength of the nonlinear interaction due to the three-to-one internal resonance weakens specifically for the indirectly excited first mode. For the single mode (second mode) response, the separation of the nontrivial stable and unstable curve decreases with decrease of the internal frequency detuning parameter.

Corresponding to various bifurcations, the system exhibits dynamic solutions namely periodic and quasiperiodic responses for typical system parameters which are illustrated with the help of time and power spectra, phase portraits and Poincare maps. The system exhibits jump phenomena for variation of control parameters.

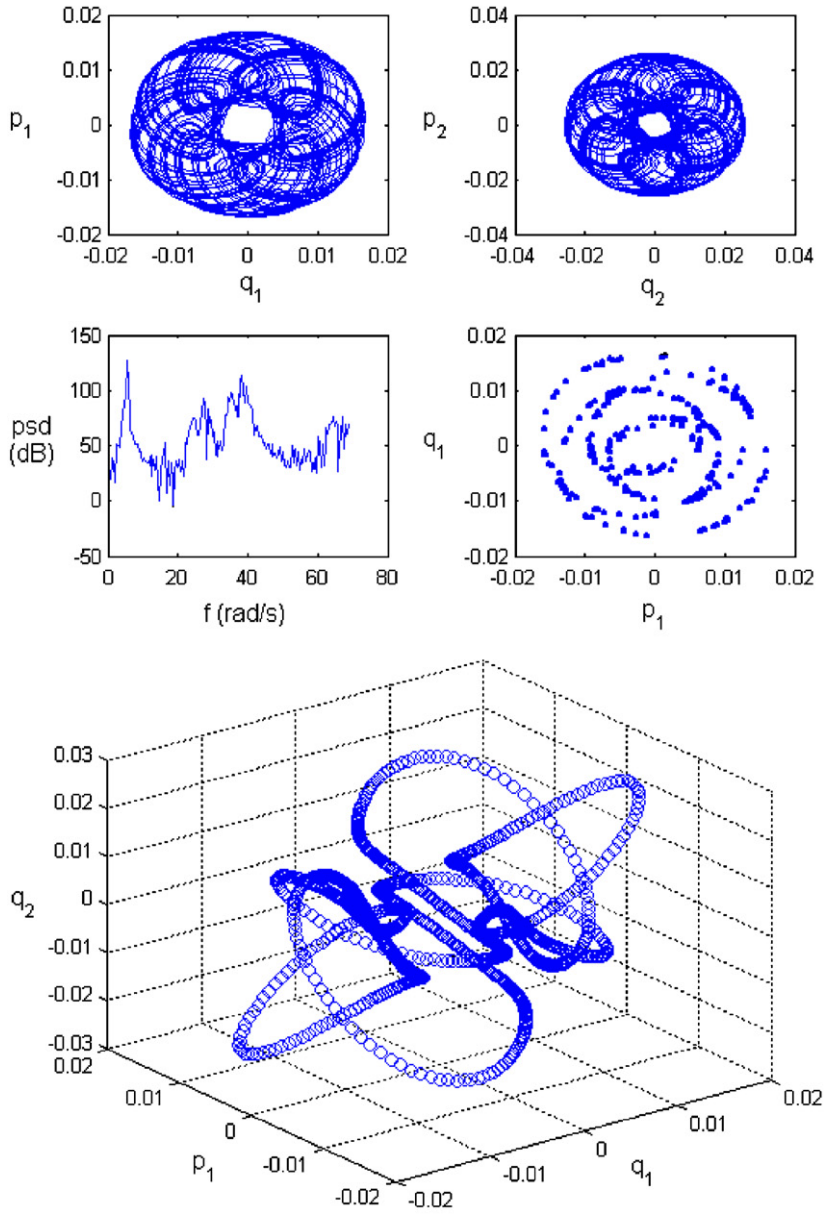

Fig. 26. Phase portrait, power spectra and Poincare map for $\sigma_2 = 183.88$, $\mu = 0.1$, $\alpha = 0$, $u_1 = 18$ and $\sigma_1 = 93.4$.

For the combination parametric resonance case, isolated two mode solutions coexist with the trivial state. There is no single mode solution. The first mode response shows monotonic increase with the increase of detuning parameter, while the second mode response decreases continuously. The system exhibits saddle node and Hopf bifurcations, jump phenomena, beating effect, periodic, quasiperiodic and chaotic responses for the chosen values of the control parameters. The route to chaos for the chosen parameters is through quasiperiodicity in the form of torus breakdown.

The trivial and nontrivial solutions of the pipe are analyzed through the direct perturbation MMS technique and a continuation algorithm. It has been demonstrated that these methods can be used for the nonlinear dynamic analysis of pipes with pulsatile flow and with internal resonance. Pipes conveying fluid being part of

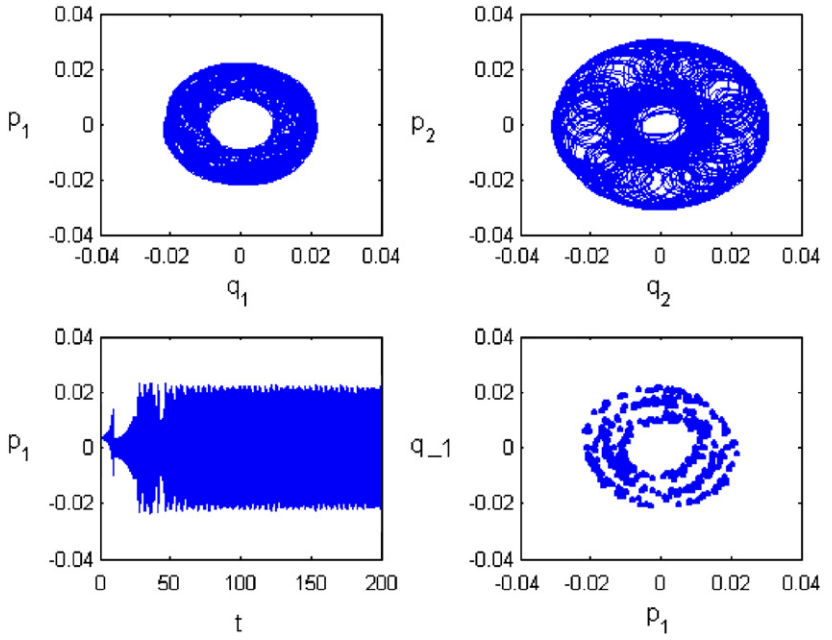

Fig. 27. Phase portrait, time history and Poincare map for $\sigma_2 = 341.72$, $\mu = 0.1$, $\alpha = 0$, $u_1 = 18$ and $\sigma_1 = 93.4$.

a broader family of traveling continua, such analysis involving internal and parametric resonances can be applied to other applications like traveling beams and strings.

Appendix

(The prime indicates derivatives of the variables corresponding to respective arguments)

$$\begin{aligned}\Gamma_1 = & -2\mathrm{i}\omega_1 A_1'\phi_1 - 2\sqrt{\beta}u_0 A_1'\phi_1' - 2\mu\mathrm{i}\omega_1 A_1\phi_1 - 2\alpha\mathrm{i}\omega_1 A_1\phi_1'''' \\ & + k\Big\{2A_1^2\bar{A}_1\phi_1''\int_0^1 \phi_1'\bar{\phi}_1'\,\mathrm{d}x + A_1^2\bar{A}_1\bar{\phi}_1''\int_0^1 \phi_1'^2\,\mathrm{d}x + 2A_1A_2\bar{A}_2\bar{\phi}_2''\int_0^1 \phi_1'\phi_2'\,\mathrm{d}x \\ & + 2A_1A_2\bar{A}_2\phi_1''\int_0^1 \phi_2'\bar{\phi}_2'\,\mathrm{d}x + 2A_1A_2\bar{A}_2\phi_2''\int_0^1 \phi_1'\bar{\phi}_2'\mathrm{d}x\Big\},\end{aligned}$$

$$\Gamma_2 = k\Big\{2\bar{A}_1^2A_2\bar{\phi}_1''\int_0^1 \phi_2'\bar{\phi}_1'\,\mathrm{d}x + \bar{A}_1^2A_2\phi_2''\int_0^1 \bar{\phi}_1'^2\,\mathrm{d}x\Big\},$$

$$\Gamma_3 = \bar{A}_1\Big\{\sqrt{\beta}u_1\omega_1\bar{\phi}_1' - \frac{\sqrt{\beta}u_1\Omega}{2}(1-\xi)\bar{\phi}_1'' + \mathrm{i}u_0u_1\bar{\phi}_1''\Big\},$$

$$\begin{aligned}\Gamma_5 = & -2\mathrm{i}\omega_2 A_2'\phi_2 - 2\sqrt{\beta}u_0 A_2'\phi_2' - 2\mu\mathrm{i}\omega_2 A_2\phi_2 - 2\alpha\mathrm{i}\omega_2 A_2\phi_2'''' \\ & + k\Big\{A_2^2\bar{A}_2\bar{\phi}_2''\int_0^1 \phi'^2_2\,\mathrm{d}x + 2A_1\bar{A}_1A_2\phi_2''\int_0^1 \phi'\bar{\phi}_1'\mathrm{d}x + 2A_1\bar{A}_1A_2\bar{\phi}_1''\int_0^1 \phi_1'\phi_2'\,\mathrm{d}x \\ & + 2A_2^2\bar{A}_2\phi_2''\int_0^1 \phi_2'\bar{\phi}_2'\,\mathrm{d}x + 2A_1\bar{A}_1A_2\phi_1''\int_0^1 \phi_2'\bar{\phi}_1'\mathrm{d}x\Big\}\end{aligned}$$

$$\Gamma_6 = kA_1^3\phi_1''\int_0^1 \phi_1'^2\,\mathrm{d}x,$$

$$\Gamma_8 = \bar{A}_2\left\{\sqrt{\beta}u_1\omega_2\bar{\phi}'_2 - \frac{\sqrt{\beta}u_1\Omega}{2}(1-\xi)\bar{\phi}''_2 + \mathrm{i}u_0u_1\bar{\phi}''_2\right\},$$

$$S_1 = \frac{\frac{k}{8}\left\{2\int_0^1 \phi''_1\bar{\phi}_1\,\mathrm{d}x\int_0^1 \phi'_1\bar{\phi}'_1\,\mathrm{d}x + \int_0^1 \bar{\phi}''_1\bar{\phi}_1\,\mathrm{d}x\int_0^1 \phi'^2_1\,\mathrm{d}x\right\}}{-\left\{\mathrm{i}\omega_1\int_0^1 \phi_1\bar{\phi}_1\,\mathrm{d}x + \sqrt{\beta}u_0\int_0^1 \phi'_1\bar{\phi}_1\,\mathrm{d}x\right\}},$$

$$S_2 = \frac{\frac{k}{4}\left\{\int_0^1 \bar{\phi}''_2\bar{\phi}_1\,\mathrm{d}x\int_0^1 \phi'_1\phi'_2\,\mathrm{d}x + \int_0^1 \phi''_1\bar{\phi}_1\,\mathrm{d}x\int_0^1 \phi'_2\bar{\phi}'_2\,\mathrm{d}x + \int_0^1 \phi''_2\bar{\phi}_1\,\mathrm{d}x\int_0^1 \phi'_1\bar{\phi}'_2\,\mathrm{d}x\right\}}{-\left\{\mathrm{i}\omega_1\int_0^1 \phi_1\bar{\phi}_1\,\mathrm{d}x + \sqrt{\beta}u_0\int_0^1 \phi'_1\bar{\phi}_1\,\mathrm{d}x\right\}},$$

$$S_3 = \frac{\frac{k}{4}\left\{\int_0^1 \phi''_2\bar{\phi}_2\,\mathrm{d}x\int_0^1 \phi'_1\bar{\phi}'_1\,\mathrm{d}x + \int_0^1 \bar{\phi}''_1\bar{\phi}_2\,\mathrm{d}x\int_0^1 \phi'_1\phi'_2\,\mathrm{d}x + \int_0^1 \phi''_1\bar{\phi}_2\,\mathrm{d}x\int_0^1 \phi'_2\bar{\phi}'_2\,\mathrm{d}x\right\}}{-\left\{\mathrm{i}\omega_2\int_0^1 \phi_2\bar{\phi}_2\,\mathrm{d}x + \sqrt{\beta}u_0\int_0^1 \phi'_2\bar{\phi}_2\,\mathrm{d}x\right\}},$$

$$S_4 = \frac{\frac{k}{8}\left\{2\int_0^1 \phi''_2\bar{\phi}_2\,\mathrm{d}x\int_0^1 \phi'_2\bar{\phi}'_2\,\mathrm{d}x + \int_0^1 \bar{\phi}''_2\bar{\phi}_2\,\mathrm{d}x\int_0^1 \phi'^2_2\,\mathrm{d}x\right\}}{-\left\{\mathrm{i}\omega_2\int_0^1 \phi_2\bar{\phi}_2\,\mathrm{d}x + \sqrt{\beta}u_0\int_0^1 \phi'_2\bar{\phi}_2\,\mathrm{d}x\right\}},$$

$$H_4 = \frac{\frac{1}{2}\left\{\sqrt{\beta}u_1\omega_2\int_0^1 \bar{\phi}'_2\bar{\phi}_1\,\mathrm{d}x - \frac{\sqrt{\beta}u_1\Omega}{2}\int_0^1(1-\xi)\bar{\phi}''_2\bar{\phi}_1\,\mathrm{d}x + \mathrm{i}u_0u_1\int_0^1 \bar{\phi}''_2\bar{\phi}_1\,\mathrm{d}x\right\}}{-\left\{\mathrm{i}\omega_1\int_0^1 \phi_1\bar{\phi}_1\,\mathrm{d}x + \sqrt{\beta}u_0\int_0^1 \phi'_1\bar{\phi}_1\,\mathrm{d}x\right\}},$$

$$H_5 = \frac{\frac{1}{2}\left\{\sqrt{\beta}u_1\omega_1\int_0^1 \bar{\phi}'_1\bar{\phi}_2\,\mathrm{d}x - \frac{\sqrt{\beta}u_1\Omega}{2}\int_0^1(1-\xi)\bar{\phi}''_1\bar{\phi}_2\,\mathrm{d}x + \mathrm{i}u_0u_1\int_0^1 \bar{\phi}''_1\bar{\phi}_2\,\mathrm{d}x\right\}}{-\left\{\mathrm{i}\omega_2\int_0^1 \phi_2\bar{\phi}_2\,\mathrm{d}x + \sqrt{\beta}u_0\int_0^1 \phi'_2\bar{\phi}_2\,\mathrm{d}x\right\}},$$

$$H_6 = \frac{\frac{1}{2}\left\{\sqrt{\beta}u_1\omega_2\int_0^1 \bar{\phi}'_2\bar{\phi}_2\,\mathrm{d}x - \frac{\sqrt{\beta}u_1\Omega}{2}\int_0^1(1-\xi)\bar{\phi}''_1\bar{\phi}_2\,\mathrm{d}x + \mathrm{i}u_0u_1\int_0^1 \bar{\phi}''_1\bar{\phi}_2\,\mathrm{d}x\right\}}{-\left\{\mathrm{i}\omega_2\int_0^1 \phi_2\bar{\phi}_2\,\mathrm{d}x + \sqrt{\beta}u_0\int_0^1 \phi'_2\bar{\phi}_2\,\mathrm{d}x\right\}},$$

$$G_1 = \frac{\frac{k}{16}\left\{2\int_0^1 \bar{\phi}''_1\bar{\phi}_1\,\mathrm{d}x\int_0^1 \phi'_2\bar{\phi}'_1\,\mathrm{d}x + \int_0^1 \phi''_2\bar{\phi}_1\,\mathrm{d}x\int_0^1 \bar{\phi}'^2_1\,\mathrm{d}x\right\}}{-\left\{\mathrm{i}\omega_1\int_0^1 \phi_1\bar{\phi}_1\,\mathrm{d}x + \sqrt{\beta}u_0\int_0^1 \phi'_1\bar{\phi}_1\,\mathrm{d}x\right\}},$$

$$G_2 = \frac{\frac{k}{16}\left\{\int_0^1 \phi''_1\bar{\phi}_2\,\mathrm{d}x\int_0^1 \phi'^2_2\,\mathrm{d}x\right\}}{-\left\{\mathrm{i}\omega_2\int_0^1 \phi_2\bar{\phi}_2\,\mathrm{d}x + \sqrt{\beta}u_0\int_0^1 \phi'_2\bar{\phi}_2\,\mathrm{d}x\right\}},$$

$$C_1 = \frac{\mathrm{i}\omega_1\int_0^1 \phi_1\bar{\phi}_1\,\mathrm{d}x}{\left\{\mathrm{i}\omega_1\int_0^1 \phi_1\bar{\phi}_1\,\mathrm{d}x + \sqrt{\beta}u_0\int_0^1 \phi'_1\bar{\phi}_1\,\mathrm{d}x\right\}},$$

$$C_2 = \frac{\mathrm{i}\omega_2\int_0^1 \phi_2\bar{\phi}_2\,\mathrm{d}x}{\left\{\mathrm{i}\omega_2\int_0^1 \phi_2\bar{\phi}_2\,\mathrm{d}x + \sqrt{\beta}u_0\int_0^1 \phi'_2\bar{\phi}_2\,\mathrm{d}x\right\}},$$

$$e_1 = \frac{i\omega_1 \int_0^1 \phi_1'''' \bar{\phi}_1 \, dx}{\left\{ i\omega_1 \int_0^1 \phi_1 \bar{\phi}_1 \, dx + \sqrt{\beta} u_0 \int_0^1 \phi_1' \bar{\phi}_1 \, dx \right\}},$$

$$e_2 = \frac{i\omega_2 \int_0^1 \phi_2'''' \bar{\phi}_2 \, dx}{\left\{ i\omega_2 \int_0^1 \phi_2 \bar{\phi}_2 \, dx + \sqrt{\beta} u_0 \int_0^1 \phi_2' \bar{\phi}_2 \, dx \right\}},$$

References

[1] M.P. Paidoussis, Flow-induced instabilities of cylindrical structures, *Applied Mechanics Review* 40 (1987) 163–175.
[2] M.P. Paidoussis, G.X. Li, Pipes conveying fluid: a model dynamical problem, *Journal of Fluids and Structures* 7 (1993) 137–204.
[3] M.P. Paidoussis, *Fluid–Structure Interactions: Slender structures and Axial flow*, Vol. 1, Academic Press, London, 1998.
[4] S.S. Chen, Dynamic stability of a tube conveying fluid, *ASCE Journal of Engineering Mechanics* 97 (1971) 1469–1485.
[5] M.P. Paidoussis, N.T. Issid, Dynamic stability of pipes conveying fluid, *Journal of Sound and Vibration* 33 (1974) 267–294.
[6] M.P. Paidoussis, C. Sundararajan, Parametric and combination resonances of a pipe conveying pulsating fluid, *ASME Journal of Applied Mechanics* 42 (1975) 780–784.
[7] J. Ginsberg, The dynamic stability of a pipe conveying a pulsatile flow, *International Journal of Engineering Science* 11 (1973) 1013–1024.
[8] S.T. Ariaratnam, N.S. Namachchivaya, Dynamic stability of pipes conveying pulsating fluid, *Journal of Sound and Vibration* 107 (1986) 215–230.
[9] N.S. Namachchivaya, Nonlinear dynamics of supported pipe conveying pulsating fluid 1. Subharmonic resonance, *International Journal of Non-Linear Mechanics* 24 (3) (1989) 185–196.
[10] N.S. Namachchivaya, W.M. Tien, Nonlinear dynamics of supported pipe conveying pulsating fluid 2. Combination resonance, *International Journal of Non-Linear Mechanics* 24 (3) (1989) 197–208.
[11] K. Jayaraman, S. Narayanan, Chaotic oscillators in pipes conveying pulsating fluid, *Nonlinear Dynamics* 10 (1996) 333–357.
[12] C.O. Chang, K.C. Chen, Dynamics and stability of pipes conveying fluid, *ASME Journal of Pressure Vessel Technology* 116 (1994) 57–66.
[13] M. Yoshizawa, H. Nao, E. Hasegawa, Y. Tsujioka, Lateral vibration of a flexible pipe conveying fluid with pulsating flow, *Bulletin of JSME* 29 (1986) 2243–2250.
[14] A.L. Thurman, C.D. Mote Jr., Non-linear oscillation of a cylinder containing flowing fluid, *ASME Journal of Engineering for Industry* 91 (1969) 1147–1155.
[15] P.J. Holmes, Bifurcations to divergence and flutter in flow-induced oscillations: a finite-dimensional analysis, *Journal of Sound and Vibration* 53 (4) (1977) 471–503.
[16] P.J. Holmes, J.E. Marsden, Bifurcation to divergence and flutter in flow- induced oscillations: an infinite dimensional analysis, *Automatica* 14 (1978) 367–384.
[17] J. Rousselet, G. Hermann, Flutter of articulated pipes at finite amplitude, *Journal of Applied Mechanics* 44 (1977) 154–158.
[18] A.K. Bajaj, P.R. Sethna, T.S. Lundgren, Hopf bifurcation phenomena in tubes carrying fluid, *SIAM Journal of Applied Mathematics* 39 (1980) 213–230.
[19] A.K. Bajaj, P.R. Sethna, Bifurcations in three dimensional motions of articulated tubes. Part 2: Non-linear analysis, *Journal of Applied Mechanics* 49 (1982) 612–618.
[20] A.K. Bajaj, P.R. Sethna, Flow induced bifurcations to three-dimensional oscillatory motions in continuous tubes, *SIAM Journal of Applied Mathematics* 44 (1984) 270–286.
[21] H.R. Oz, H. Boyaci, Transverse vibrations of tensioned pipes conveying fluid with time-dependent velocity, *Journal of Sound and Vibration* 236 (2) (2000) 259–276.
[22] H.R. Oz, Nonlinear vibrations and stability analysis of tensioned pipes conveying fluid with variable velocity, *International Journal of Non-Linear Mechanics* 36 (1) (2001) 1031–1039.
[23] H.R. Oz, M. Pakdemirli, H. Boyaci, Nonlinear vibrations and stability of an axially moving beam with time-dependent velocity, *International Journal of Non-Linear Mechanics* 36 (1) (2001) 107–115.
[24] A.H. Nayfeh, J.F. Nayfeh, D.T. Mook, On methods for continuous systems with quadratic and cubic nonlinearities, *Nonlinear Dynamics* 3 (1992) 145–162.
[25] M. Pakdemirli, A comparison of two perturbation methods for vibration of systems with quadratic and cubic nonlinearities, *Mechanics Research Communications* 21 (1994) 203–208.
[26] M. Pakdemirli, H. Boyaci, Comparison of direct-perturbation methods with discretization-perturbation methods for nonlinear vibrations, *Journal of Sound and Vibration* 186 (1995) 837–845.
[27] E.G. Tezak, D.T. Mook, A.H. Nayfeh, Nonlinear analysis of the lateral response of columns to periodic loads, *Journal of Mechanical Design* 100 (1978) 651–659.
[28] C.M. Chin, A.H. Nayfeh, Three-to-one internal resonances in parametrically excited hinged-clamped beams, *Nonlinear Dynamics* 20 (1999) 131–158.

[29] A.H. Nayfeh, B. Balachandran, Modal Interactions in Dynamical and Structural Systems, *Applied Mechanics Review* 42 (1989) 175–201.
[30] A.H. Nayfeh, *Nonlinear Interactions*, Wiley, New York, 1998.
[31] A.H. Nayfeh, D.T. Mook, *Nonlinear Oscillations*, Wiley, New York, 1979.
[32] A.H. Nayfeh, B. Balachandran, *Applied Nonlinear Dynamics: analytical computational and Experimental Methods*, Wiley-Interscience, New York, 1995.